Article

Developmental Cell

MEIOSIN Directs the Switch from Mitosis to Meiosis in Mammalian Germ Cells

Graphical Abstract

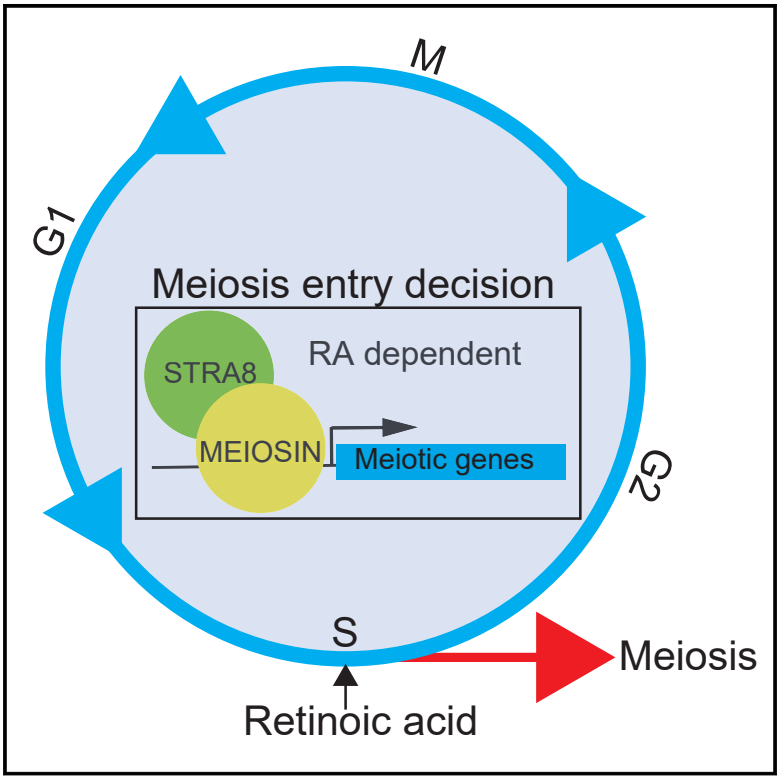

Authors

Kei-ichiro Ishiguro, Kumi Matsuura, Naoki Tani, ..., Minoru S.H. Ko, Kimi Araki, Hitoshi Niwa

Correspondence

ishiguro@kumamoto-u.ac.jp

In Brief

Although meiosis is a fundamental and well-studied biological process, the molecular mechanisms regulating its initiation are poorly understood. Ishiguro et al. identify MEIOSIN as a key initiator of meiosis and elucidate a framework for understanding how switching of the cell cycle from mitosis to meiosis occurs in the mammalian germline.

Highlights

- MEIOSIN plays an essential role in meiotic initiation both in male and female
- MEIOSIN and STRA8 bind and activate meiotic genes
- MEIOSIN and STRA8 play a central role in cell-cycle switching from mitosis to meiosis
- Temporal expression of MEIOSIN is required for meiotic entry decision

Ishiguro et al., 2020, Developmental Cell *52*, 429–445
February 24, 2020
https://doi.org/10.1016/j.devcel.2020.01.010

CellPress

Developmental Cell
Article

MEIOSIN Directs the Switch from Mitosis to Meiosis in Mammalian Germ Cells

Kei-ichiro Ishiguro,[1,7,*] Kumi Matsuura,[2] Naoki Tani,[3] Naoki Takeda,[4] Shingo Usuki,[3] Mariko Yamane,[2] Michihiko Sugimoto,[4] Sayoko Fujimura,[3] Mihoko Hosokawa,[5] Shinichiro Chuma,[5] Minoru S.H. Ko,[6] Kimi Araki,[4] and Hitoshi Niwa[2]

[1]Department of Chromosome Biology, Institute of Molecular Embryology and Genetics (IMEG), Kumamoto University, Kumamoto 860-0811, Japan
[2]Department of Pluripotent Stem Cell Biology, IMEG, Kumamoto University, Kumamoto 860-0811, Japan
[3]Liaison Laboratory Research Promotion Center, IMEG, Kumamoto University, Kumamoto 860-0811, Japan
[4]Institute of Resource Development and Analysis, Kumamoto University, Kumamoto 860-0811, Japan
[5]Laboratory of Developmental Epigenome, Institute for Frontier Life and Medical Sciences, Kyoto University 606-8507, Japan
[6]Department of Systems Medicine, Keio University School of Medicine 160-8582, Japan
[7]Lead Contact
*Correspondence: ishiguro@kumamoto-u.ac.jp
https://doi.org/10.1016/j.devcel.2020.01.010

SUMMARY

The mechanisms regulating meiotic initiation in mammals are enigmatic. It is known that retinoic acid (RA) signaling plays a pivotal role during meiotic initiation. STRA8, which is expressed in response to RA, is thought to be a key factor promoting meiotic initiation. However, the specific role of STRA8 in meiotic initiation has remained elusive. Here, we identified MEIOSIN as a germ-cell-specific factor that associates with STRA8. MEIOSIN, like STRA8, is expressed in response to RA and plays an essential role in meiotic initiation in both males and females. Functional analyses revealed that MEIOSIN acts as a transcription factor together with STRA8, and that both factors are critical for driving meiotic gene activation. Furthermore, temporally restricted expression of MEIOSIN leads to meiotic entry decision during spermatogenesis. The present study demonstrates that MEIOSIN, in collaboration with STRA8, plays a central role in regulating the mitosis to meiosis germ cell fate decision in mammals.

INTRODUCTION

In eukaryotic cell division, genomic information is equally transferred to daughter cells in mitosis, whereas it is halved in meiosis. The meiotic cell cycle consists of one round of DNA replication at pre-meiotic S phase followed by two rounds of chromosome segregation, producing haploid gametes from diploid cells. Meiotic prophase I is a specialized stage that is equivalent to G2 phase of the canonical cell cycle, which is prolonged to ensure the completion of numerous meiosis-specific chromosome events (Baudat et al., 2013; Cahoon and Hawley, 2016; Handel and Schimenti, 2010; Page and Hawley, 2004; Zickler and Kleckner, 2015). In mouse, retinoic acid (RA) induces meiotic transcription (Bowles et al., 2006; Koubova et al., 2006) via both *Stra8* (stimulated by RA gene 8)-dependent (Baltus et al., 2006) and -independent (Koubova et al., 2014; Soh et al., 2015) mechanisms. STRA8 is expressed at the preleptotene stage in the embryonic ovary (Menke et al., 2003) and in the postnatal testis prior to entry into the meiotic prophase I (Oulad-Abdelghani et al., 1996). Since germ cells fail to undergo normal meiosis in *Stra8* deficient male and female mice (Anderson et al., 2008; Baltus et al., 2006; Dokshin et al., 2013; Mark et al., 2008), it is widely believed that STRA8 plays a crucial role in the progression of meiosis. However, the exact role of STRA8 in meiosis remains elusive. Recently, it was shown that STRA8 binds to and activates not only meiotic genes but also a wide variety of cell cycle genes that are not restricted to meiosis (Kojima et al., 2019). Also, it has been argued that whereas *Stra8* deficient cells do not undergo pre-meiotic S phase in C57BL/6 background (Baltus et al., 2006; Anderson et al., 2008), those in mixed genetic background initiates but fails to complete meiotic prophase I (Mark et al., 2008), suggesting whether STRA8 is involved in the initiation of meiosis depends on genetic backgrounds. Furthermore, in testis, STRA8 is also transiently expressed in differentiating spermatogonia (Mark et al., 2008; Endo et al., 2015; Zhou et al., 2008) far before the differentiation into preleptotene spermatocytes. It is a large enigma why initiation of meiosis occurs only in preleptotene spermatocytes, the second time of STRA8 expression, but not in spermatogonia despite the expression of STRA8 (Mark et al., 2008; Endo et al., 2015; Zhou et al., 2008). Thus, whether STRA8 is indeed required for meiotic initiation has been controversial. In addition to RA signaling, DAZL (Lin et al., 2008) and BMP (Miyauchi et al., 2017) synergistically contribute to meiotic initiation. Also, it has been suggested that meiotic entry is negatively regulated by DMRT1 (Matson et al., 2010) and MAX (Suzuki et al., 2016). Thus, multiple layers of regulation may underlie the commitment to meiotic initiation. Although STRA8 is thought to be one of the key regulators for meiosis, the entire molecular mechanism of meiotic initiation is a longstanding unsolved question. Here, we report MEIOSIN, a STRA8-interacting protein that we identified, should shed light to this question.

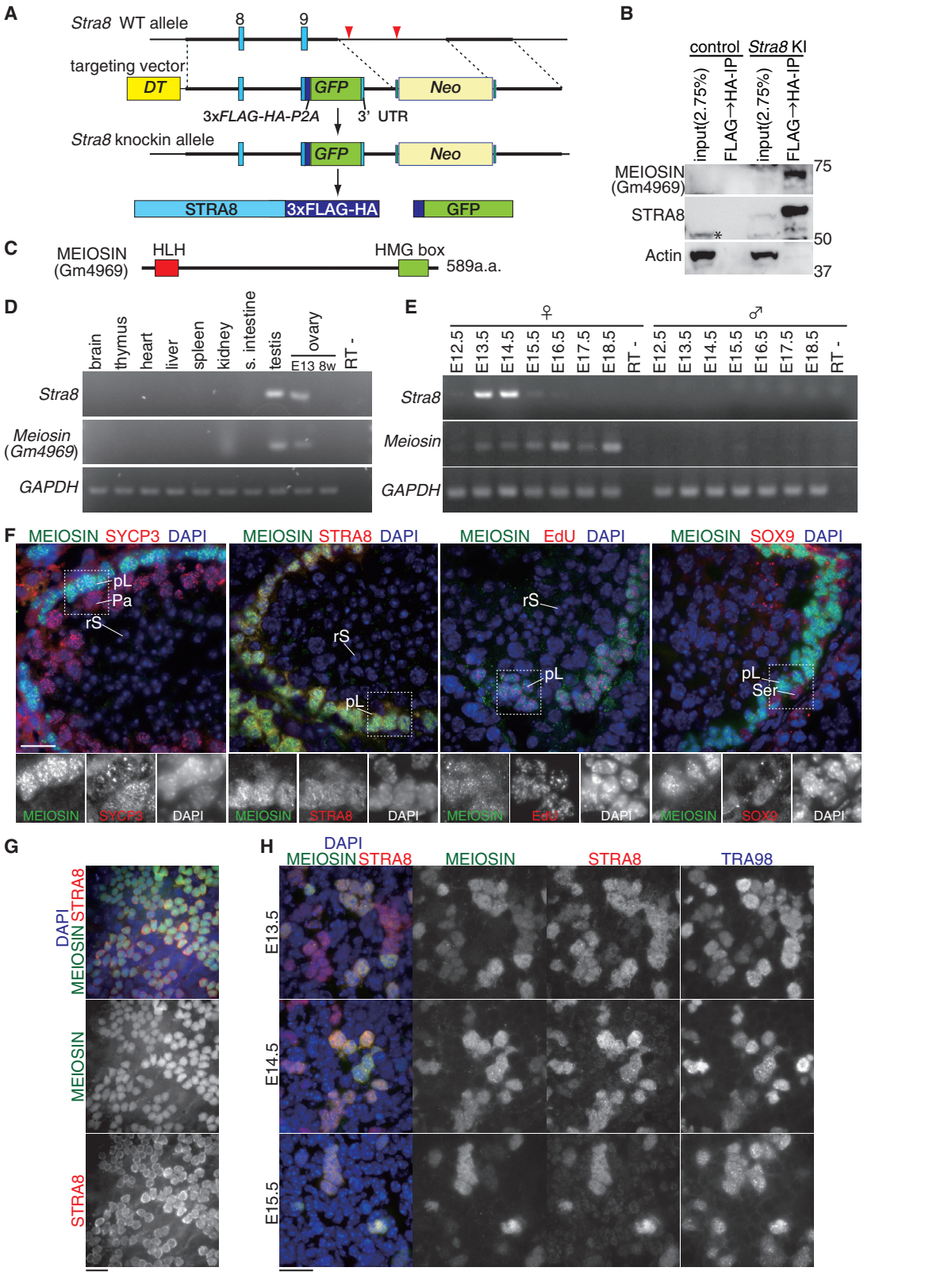

(legend on next page)

RESULTS

Identification of MEIOSIN, a STRA8-Interacting Protein

To elucidate the molecular mechanism of meiotic initiation, we investigated STRA8-interacting proteins through immunoprecipitation (IP) of STRA8 from chromatin extracts of mouse testes. For this purpose, we generated *Stra8-3xFLAG-HA-p2A-GFP* knockin (KI) (*Stra8-3FH-GFP* KI) mice (Figures 1A and S1A–S1C), which allowed tandem IPs using anti-FLAG and anti-HA antibodies. Mass spectrometry (MS) analysis of the immunoprecipitates identified a protein encoded by the hypothetical gene *Gm4969*. The same protein was reproducibly identified also in anti-STRA8 IP from wild-type (WT) testes (Figure S1D). This protein was named MEIOSIN (meiosis initiator) after its *in vivo* function described later. IP followed by western blotting using chromatin extracts from the *Stra8-3FH-GFP* KI testes indicated that MEIOSIN indeed forms a complex with STRA8 (Figure 1B). A similar result was obtained by MS analysis of immunoprecipitates from the chromatin-unbound fraction of *Stra8-3FH-GFP* KI testes (Figure S1E), suggesting that the MEIOSIN-STRA8 interaction may occur in a DNA-independent manner. Prediction of the amino acid sequence of MEIOSIN revealed that it possesses basic helix-loop-helix (HLH) and high mobility group (HMG) box domains, implying its role as a DNA binding protein (Figures 1C and S2). BLAST search analysis revealed that MEIOSIN is conserved in vertebrates (Figure S2). The *Meiosin* gene showed a specific expression in adult testis and embryonic ovary but not in other adult organs (Figure 1D), suggesting that MEIOSIN is a germ cell-specific factor similar to STRA8. Although the expressions of *Meiosin* and *Stra8* are both induced in the early stages (embryonic day [E]13.5) in the embryonic ovary but not in embryonic testis, the mRNA of *Meiosin*, unlike that of *Stra8*, persisted throughout the period of female meiosis (Figure 1E).

MEIOSIN Is Expressed at the Initiation of Meiosis in the Testis and Ovary

To determine the meiotic stage or cell type-specific expression of MEIOSIN, the seminiferous tubules of the testes were immunostained with specific antibodies against MEIOSIN along with STRA8 and SYCP3, a component of meiotic axial element (AE) (Figure 1F). While STRA8 was observed in the cytoplasm and the nuclei, MEIOSIN was localized mostly in the nuclei of the spermatocytes during the preleptotene stage in the stage VII–VIII seminiferous tubules, largely colocalizing with STRA8 (Figures 1F and S1F). However, it was not observed in spermatocytes at other stages, postmeiotic spermatids, spermatogonia, or Sertoli cells (SOX9 expressing cells) (Figure 1F). The timing of MEIOSIN expression overlapped with meiotic DNA replication, as shown by EdU incorporation occurring in a subpopulation of MEIOSIN positive cells (32.3%~42.1% of the seminiferous tubules that have EdU/MEIOSIN double positive cells per total number of the seminiferous tubules that have MEIOSIN positive cells) (Figure 1F). Whole mount immunostaining of the seminiferous tubules showed that MEIOSIN/STRA8 double positive cells were observed in a limited area along the tubules, suggesting that temporal expression of MEIOSIN is regulated in the seminiferous tubule cycles, like STRA8 (Figure 1G). In females, TRA98 is a marker that distinguishes germ cells from somatic cells in embryonic ovary (Liu et al., 2010). MEIOSIN was expressed in the TRA98 positive germ cells of embryonic ovary during E13.5 -15.5 at the time of meiotic initiation (Figure 1H). Although the expression of *Meiosin* mRNA persists beyond E13.5 (Figure 1E), the number of MEIOSIN-positive cells culminated during E13.5–E14.5 with gradual reduction at E15.5, like STRA8. This implies the expression of MEIOSIN is post-transcriptionally regulated upon the entry into meiotic prophase I. Taken together, these results suggest that MEIOSIN is transiently coexpressed with STRA8 at the entry into the meiotic prophase I both in male and female germ cells.

MEIOSIN Is Required for Progression of Meiosis

In order to address the role of MEIOSIN in germ cells, we deleted Exon6-Exon14 of *Meiosin* loci in C57BL/6 fertilized eggs with the CRISPR/Cas9 system (Figures 2A and 2B).

Although *Meiosin* knockout (KO) mice developed normally, defects in reproductive organs were evident with smaller-than-normal testes (Figure 2C). Histological analysis revealed severely impaired spermatogenesis and the absence of postmeiotic spermatids or sperm in 8-week-old *Meiosin* KO testes and epididymis (Figures 2D–2F). In *Meiosin* KO testes, STRA8 was expressed and vice versa (Figure 2G; see also Figure S3), implying that the expressions of *Meiosin* and *Stra8* are regulated independently of each other. Notably, spermatocytes later than the preleptotene-like stage did not appear in *Meiosin* KO mice at postnatal day (P)18, when the first wave of

Figure 1. Identification of the Germ Cell-Specific Factor MEIOSIN

Figure360▷ For a Figure360 author presentation of this figure, see https://doi.org/10.1016/j.devcel.2020.01.010.

(A) Schematic illustrations of the *Stra8* WT allele and the *3xFLAG-HA-p2A-GFP* KI allele. Blue boxes represent exons. Coding exon 9 is followed by *3xFLAG-HA-p2A-GFP* and the 3′UTR. Triangles (red): CRISPR gRNA target sites. DT: diphtheria toxin gene. Neo: neomycin resistance gene. The dashed lines indicate 5′ and 3′ homology between the targeting vector and the *Stra8* locus.

(B) Western blot showed immunoprecipitates after tandem affinity purifications using anti-FLAG and anti-HA from chromatin extracts of WT (non-tagged control) and KI mouse testes. *: endogenous STRA8. Note that anti-STRA8 blot detected 3xFLAG-HA tagged STRA8 at higher molecular weight than the endogenous STRA8.

(C) A schematic illustration of the putative protein encoded by *Gm4969*.

(D) The tissue-specific expression pattern of *Meiosin* (*Gm4969*) was examined using RT-PCR. Testis RNA was obtained from 8-week-old male mice. Ovary RNA was obtained from embryonic day 13 and adult 8-week-old female mice. RT- indicates control PCR without reverse transcription.

(E) The expression pattern of *Meiosin* in the embryonic ovary and testis was examined using RT-PCR.

(F) Seminiferous tubule sections from adult WT testes (8-week-old) were stained as indicated. Enlarged images are shown on the bottom. EdU was injected for 2 h pL, preleptotene spermatocyte; Pa, pachytene spermatocyte; rS, round spermatid; Ser, Sertoli cell.

(G) Whole mount immunostaining of the seminiferous tubules as indicated.

(H) Embryonic ovary sections were stained as indicated along with a germ cell marker, TRA98. Scale bars: 25 μm.

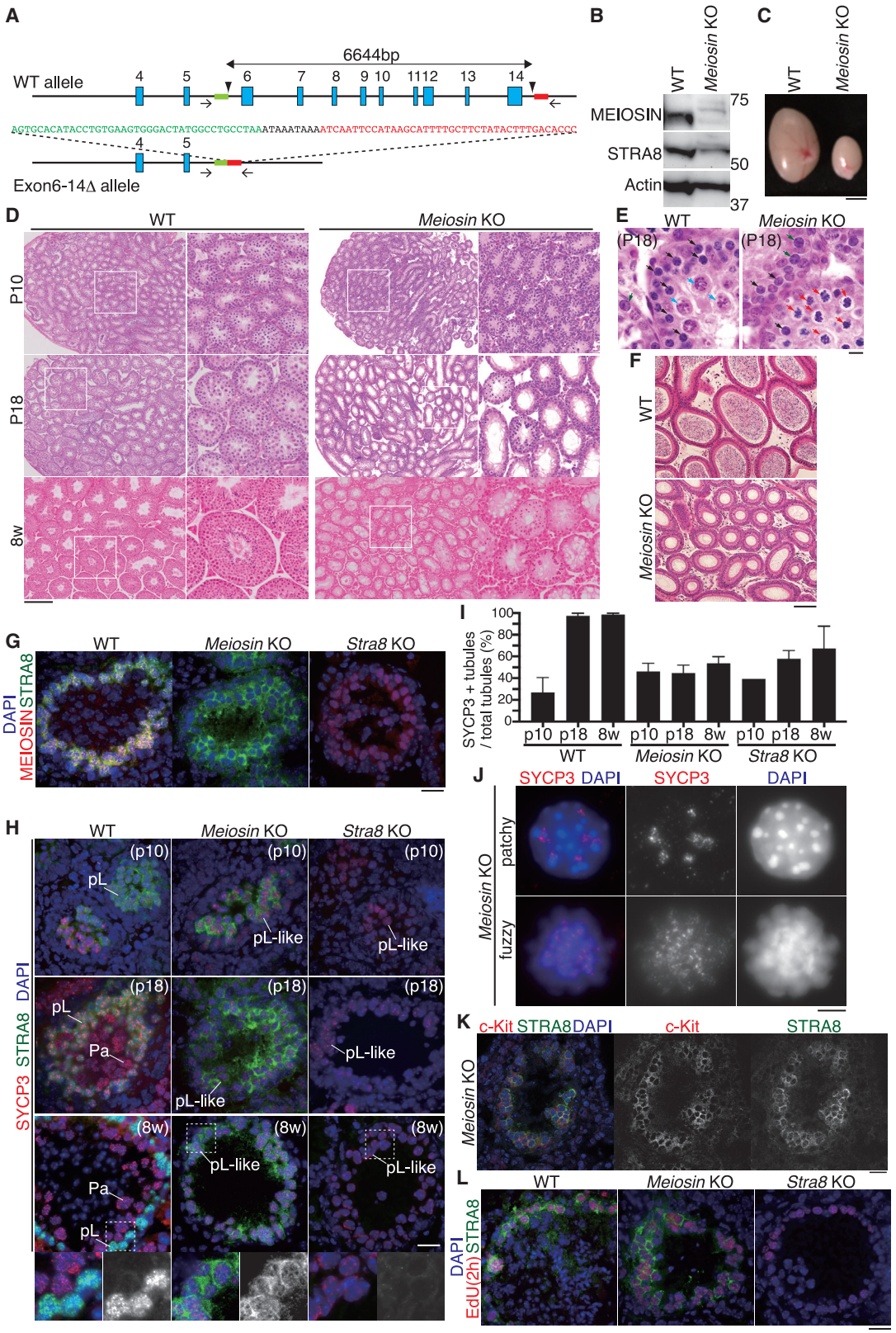

Figure 2. MEIOSIN Is Required for Progression of Meiosis

(A) The targeted Exon6–14 deletion allele of *Meiosin* were generated by the introduction of CAS9, synthetic gRNAs designed to target intron5 and the downstream of Exon14 (arrowheads), and ssODN into the C57BL/6 fertilized eggs. Arrows: PCR primer sites for genotyping.

(legend continued on next page)

spermatogenesis reached pachytene stage meiotic prophase in wild type (Figures 2H and 2I). The phenotype persisted through adulthood in *Meiosin* KO mice (Figure 2H). Hence, the primary defect had already occurred at the meiotic entry rather than during the meiotic prophase. Most of the *Meiosin* KO spermatocyte-like cells showed a preleptotene-like morphology with patchy aggregates of SYCP3 or fuzzy SYCP3 pattern (Figure 2J), suggesting that the AE formation was incomplete (discussed later, see Figure 3C). Thus, despite the expression of STRA8, *Meiosin* KO spermatocyte-like cells failed to undergo normal meiotic prophase. c-Kit positive cells appeared in *Meiosin* KO testis (Figure 2K), suggesting that spermatogonial differentiation normally occurred (Yoshinaga et al., 1991). Since spermatogenesis reached at least the preleptotene-like stage (patchy SYCP3+, EdU+, STRA8+) in *Meiosin* KO testis (Figures 2H and 2L), the observed defect occurred in the process of meiosis rather than during the differentiation of spermatogonia into spermatocytes. Overall, meiotic block observed in *Meiosin* KO mice was similar to those observed in *Stra8* KO mice (Figures 2G and 2H) and to those reported in the previous analyses of *Stra8* mutants (Anderson et al., 2008; Mark et al., 2008), except for some cytological differences in a subpopulation of *Stra8* KO testis (discussed later, see Figure 4). Surprisingly, STRA8 largely remained in the cytoplasm of *Meiosin* KO mice, whereas it was largely in the nuclei of WT (Figures 2G and 2H). MEIOSIN localized in the nuclei of *Stra8* KO mice (Figure 2G). This implies that MEIOSIN may play a role in the retention of STRA8 in the nuclei, and that lack of nuclear localization of STRA8 in preleptotene spermatocytes may result in the phenotype similarly shown both in *Meiosin* and *Stra8* KO mice. These cytological observations demonstrate that *Meiosin* KO spermatocyte-like cells fail to progress into meiosis and spermatogenesis. Thus, these results suggest that MEIOSIN is required for the progression into meiosis.

MEIOSIN Plays a Role in Cell-Cycle Switching from Mitosis to Meiosis

It was unclear whether SYCP3+ cells in *Meiosin* KO testis represented preleptotene arrest or still would show cell-cycle progression. So next, we analyzed the cell-cycle state in *Meiosin* KO. We noticed that a subpopulation of spermatocyte-like cells in *Meiosin* KO mice showed histone H3Ser10 phosphorylation (H3S10P) on the chromatin, a marker of M-phase chromosome, at earlier stages (Figure 3A), whereas H3S10P+/centromeric SYCP3+ spermatocytes appeared only at Metaphase I in WT. Consistently, similar phenomena were observed in the *Stra8* KO testis (Figure 3A) (Mark et al., 2008), albeit at a lower frequency compared to the *Meiosin* KO. In *Meiosin* KO mice, H3Ser10 phosphorylation was exclusively observed in the spermatocyte-like cells with a diffusive or fuzzy SYCP3 staining pattern (Figure 3B). Assessment of chromosome spread indicated that H3S10P/SYCP3+ cells in *Meiosin* KO showed prometaphase-like condensed chromosomes (Figure 3C). Notably, H3S10P+/SYCP3+ spermatocyte-like cells appeared as early as P10 (the time point when initial wave of meiotic entry occurs) in *Meiosin* KO testis (Figure 3A), suggesting that *Meiosin* KO spermatocyte-like cells underwent precocious mitotic status soon after they reached the preleptotene-like stage. To examine this hypothesis, we analyzed the fate of *Meiosin* KO spermatocyte-like cells by EdU labeling and chasing. EdU-labeled *Meiosin* KO spermatocyte-like cells showed the characteristics of H3S10P positive M-phase chromosomes 24 h after meiotic DNA replication, in contrast to EdU-labeled WT spermatocytes that reached only the leptotene stage that is far before Metaphase I (Figure 3D). Furthermore, MEIKIN, a meiosis I-specific kinetochore protein that is required for reductional chromosome segregation (Kim et al., 2015), was absent in the prometaphase-like chromosomes in the *Meiosin* KO and *Stra8* KO mice (Figure 3E). Thus, *Meiosin* KO preleptotene-like cells underwent mitotic chromosome condensation but did not progress through canonical meiotic prophase I. Consistent with those observations, mitotic cyclin A2 (CCNA2) was expressed in SYCP3+ cells in *Meiosin* KO testis (Figure 3F), further supporting the notion that *Meiosin* KO spermatocyte-like cells underwent mitotic cell cycle. Therefore, although *Meiosin* KO and *Stra8* KO spermatocyte-like cells partially showed a meiotic profile, they entered the mitotic status rather than having the cell-cycle arrested. Furthermore, a subpopulation of those mitotic cells was TUNEL positive, suggesting that the aberrant mitotic cells were eliminated at least in part by apoptosis (Figure 3G). Collectively, these data indicate that the MEIOSIN-STRA8 complex plays a crucial role in cell-cycle switching from mitosis to meiosis.

(B) Immunoblot analysis of testis extracts prepared from mice with the indicated genotypes (P18).
(C) Testes from WT and *Meiosin* KO (8-week-old). Scale bar: 2 mm.
(D) Hematoxylin and eosin staining of the sections from WT and *Meiosin* KO testes (P10, P18, 8-week-old). Scale bar: 250 μm. Enlarged images are shown on the right.
(E) Magnified images of hematoxylin and eosin staining of the sections from WT and *Meiosin* KO testes (P18). Scale bar: 10 μm. Black arrow, preleptotene (-like) spermatocyte; blue arrow, pachytene spermatocyte; green arrow, type B spermatogonia; red arrow, mitotic cell.
(F) Hematoxylin and eosin staining of the sections from WT and *Meiosin* KO epididymis (8-week-old). Scale bar: 100 μm.
(G) Seminiferous tubule sections from WT, *Meiosin* KO, and *Stra8* KO testes (P18) were stained for MEIOSIN, STRA8, and DAPI (DNA).
(H) Seminiferous tubule sections from WT, *Meiosin* KO, and *Stra8* KO testes (upper: P10, middle: P18, lower: 8-week-old) were stained for SYCP3, STRA8, and DAPI. Enlarged images show that STRA8 was localized mostly in the nuclei in WT testes and both in the cytoplasm and the nuclei in *Meiosin* KO testes. pL, preleptotene spermatocyte; Pa, pachytene spermatocyte.
(I) Quantification of the seminiferous tubules containing SYCP3+ spermatocyte or spermatocyte-like cells per total number of the seminiferous tubules in WT (p10: n = 2, p18: n = 4, 8W: n = 4), *Meiosin* KO (p10: n = 2, p18: n = 3, 8W: n = 5), and *Stra8* KO (p10: n = 1, p18: n = 4, 8W: n = 5) testes (bar graph with SD).
(J) Chromosome spreads of *Meiosin* KO spermatocyte-like cells were stained for SYCP3 and DAPI. Immunostaining patterns of SYCP3 are classified as patchy or fuzzy. Scale bar: 5 μm
(K) Seminiferous tubule sections from *Meiosin* KO testes (8-week-old) was stained for cKit, STRA8 and DAPI.
(L) Seminiferous tubule sections from WT and *Meiosin* KO testes (8-week-old) were stained for EdU, STRA8, and DAPI 2 h after the injection of EdU. Scale bars: 25 μm except for (C), (D), (E), (F), and (J).

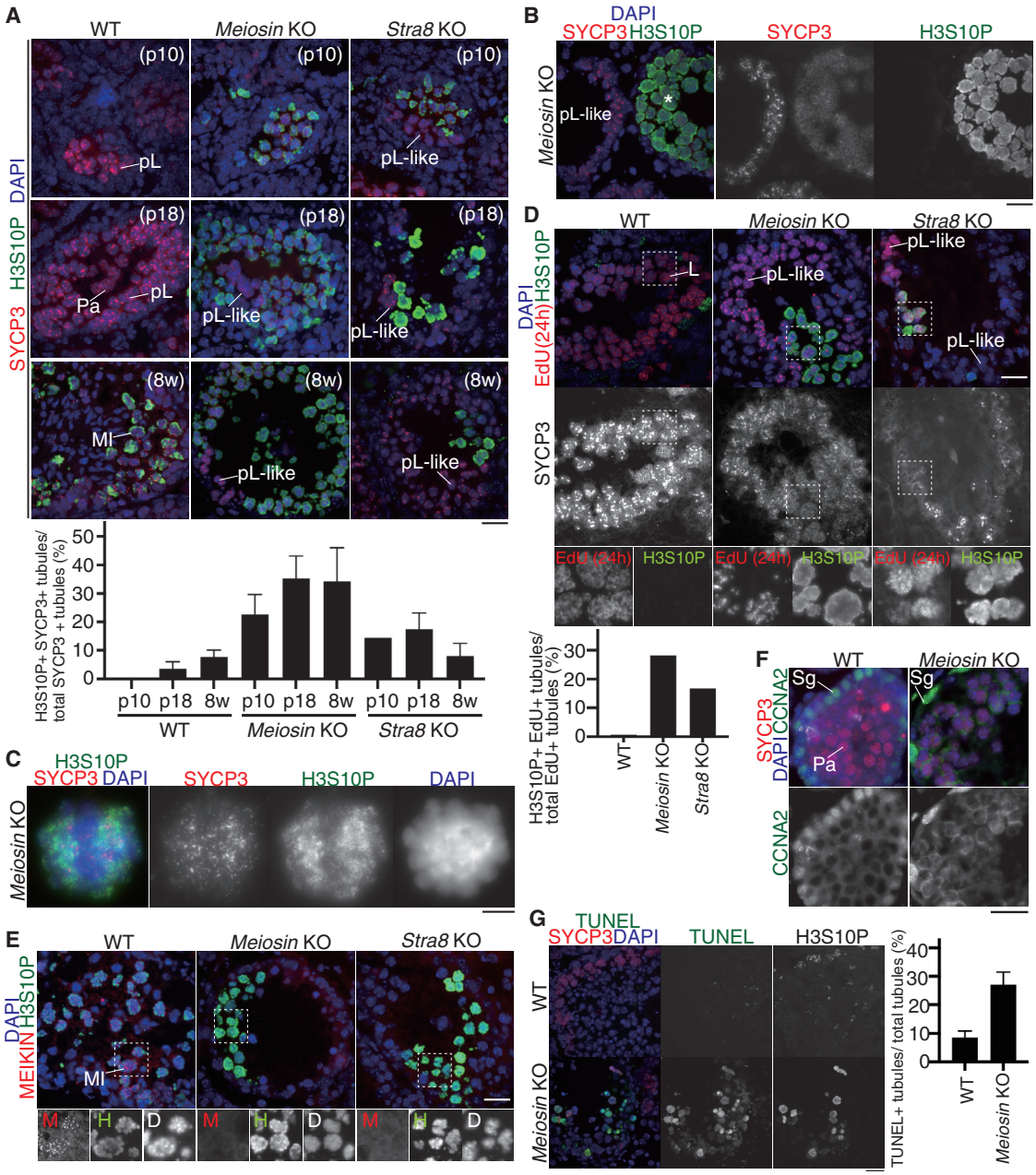

Figure 3. MEIOSIN Plays a Role in Cell-Cycle Switching from Mitosis to Meiosis

(A) Seminiferous tubule sections (upper: P10, middle: P18, lower: 8-week-old) were stained for SYCP3, H3S10P, and DAPI. MI: metaphase I, pL: preleptotene, pL-like: preleptotene-like, Pa: pachytene. Quantification of the seminiferous tubules that have H3S10P+/SYCP3+ cells per the seminiferous tubules that have SYCP3+ spermatocyte(-like) cells in WT (p10: n = 2, p18: n = 4, 8W: n = 4), *Meiosin* KO (p10: n = 2, p18: n = 3, 8W: n = 5), and *Stra8* KO (p10: n = 1, p18: n = 4, 8W: n = 5) testes (bar graph with SD). Note that H3S10P+/centromeric SYCP3+ spermatocytes correspond to metaphase I.

(B) Seminiferous tubule sections (4-week-old) in the *Meiosin* KO were stained as in (A). pL-like: preleptotene-like spermatocytes. *: diffusive SYCP3+ spermatocyte-like cells that progressed beyond preleptotene-like stage.

(C) Chromosome spreads of *Meiosin* KO spermatocyte-like cells were stained for SYCP3, H3S10P, and DAPI. Scale bar: 5 μm.

(D) Seminiferous tubule sections from WT, *Meiosin* KO, and *Stra8* KO testes (18-day-old) 24 h post EdU injection were stained for EdU, H3S10P, SYCP3, and DAPI. Enlarged images are shown. L: leptotene, pL-like: preleptotene-like. Quantification of the seminiferous tubules that have H3S10P+/EdU+ spermatocyte-like cells per the seminiferous tubules that have EdU labeled spermatocyte-like cells in WT, *Meiosin* KO, and *Stra8* KO testes (bar graph).

(E) Seminiferous tubule sections (8-week-old) were stained for H3S10P, MEIKIN, and DAPI. Enlarged images are shown on the bottom. MI: metaphase I.

(F) Seminiferous tubule sections (P18) from WT and *Meiosin* KO testes were stained for SYCP3, CCNA2, and DAPI. Pa, pachytene; sg, spermatogonia.

(G) Seminiferous tubule sections (8-week-old) were stained for SYCP3, TUNEL, H3S10P, and DAPI. Quantification of the seminiferous tubules that have TUNEL+ cells per total number of the seminiferous tubules in WT (n = 3) and *Meiosin* KO (n = 3) testes (bar graph with SD). Scale bars: 25 μm except for (C).

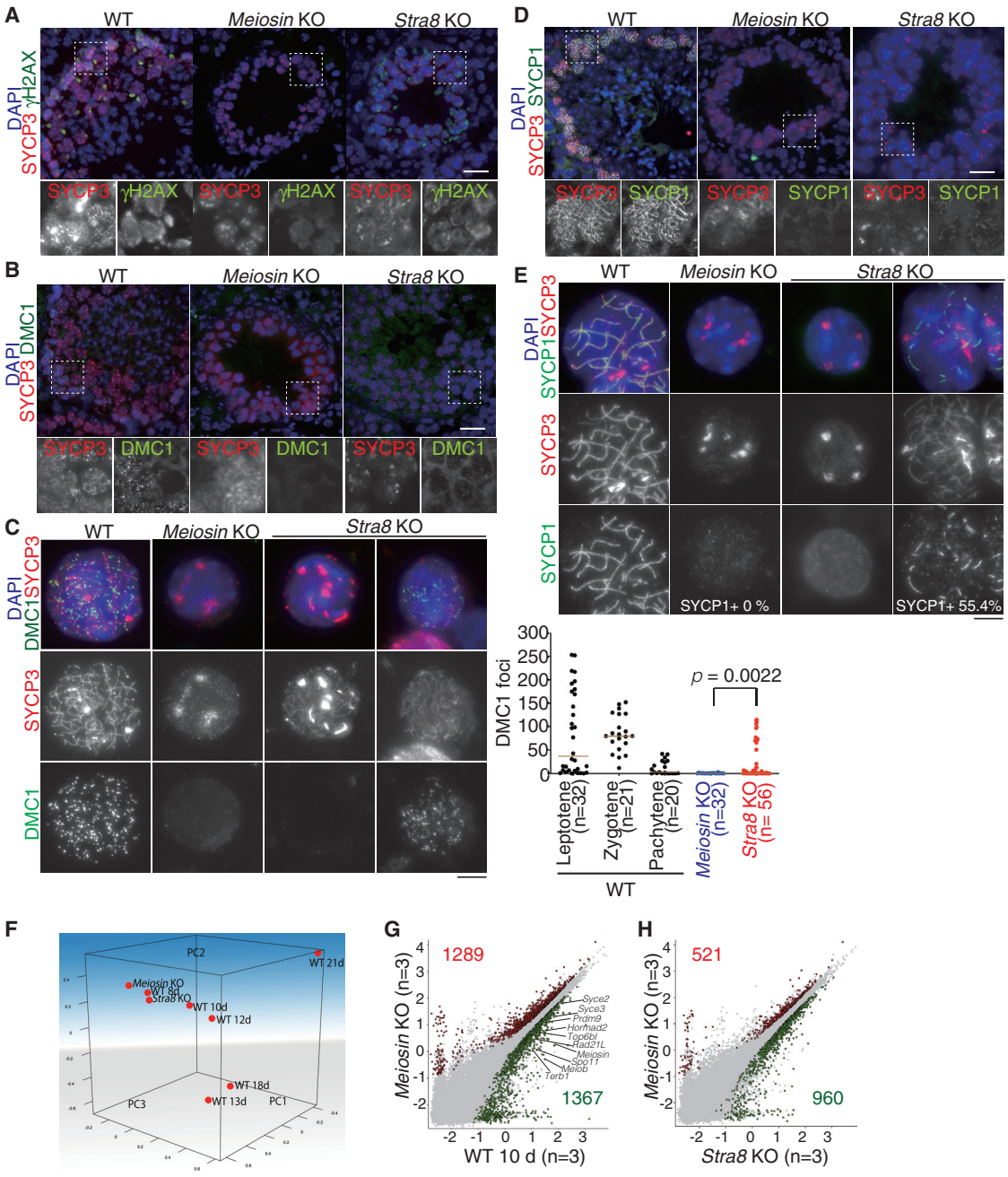

Figure 4. MEIOSIN Is Required for Meiotic Prophase Program in Male

(A) Seminiferous tubule sections (8-week-old) were stained as indicated for SYCP3, γH2AX (a marker for DSB and XY body), and DAPI. Enlarged images are shown below.

(B) Seminiferous tubule sections (8-week-old) were stained for DMC1 (a marker for meiotic recombination) as in (A).

(C) Chromosome spreads of WT spermatocytes, *Meiosin* KO, and *Stra8* KO spermatocyte-like cells were stained for SYCP3, DMC1, and DAPI (left). Numbers of DMC1 foci on SYCP3 axes are shown in the scatter plot with median (right). p value (Mann–Whitney t test) is shown.

(D) Seminiferous tubule sections (8-week-old) were stained for SYCP1 (a marker for homolog synapsis) as in (A).

(E) Chromosome spreads of WT spermatocytes, *Meiosin* KO, and *Stra8* KO spermatocyte-like cells were stained for SYCP3, SYCP1, and DAPI. Percentages of SYCP1 positive cells are shown below. Note that more extended SYCP3-stained axes, more numbers of DMC1 foci and partial synapsis were observed in *Stra8* KO spermatocyte-like cells compared to *Meiosin* KO, suggesting that *Stra8* KO spermatocyte-like cells still have the ability to undergo meiotic prophase program.

(F) PCA of the transcriptomes of WT (8, 10, 12, 13, 18, and 21 days), *Meiosin* KO (21 days), and *Stra8* KO (21 days) is shown.

(G) Scatter plot of transcriptomes of 10-day WT (n = 3) versus *Meiosin* KO (n = 3). The numbers of differentially expressed genes are shown. Significance criteria: false discovery rate $\leq$ 0.05, fold change $\geq$ 1.5.

(H) Scatter plot of transcriptomes of *Stra8* KO (n = 3) versus *Meiosin* KO (n = 3). Scale bars: 5 μm for (C) and (E). Scale bars: 25 μm for (A), (B), and (D).

MEIOSIN Is Required for Meiotic Prophase Program in Male

We sought the causal effect that gives preleptotene-like morphologies to the cells in *Meiosin* KO testis by more advanced stage markers such as γH2AX for DNA double strand break (DSB) (Hamer et al., 2003), DMC1 for intermediates of meiotic recombination (Pittman et al., 1998; Yoshida et al., 1998), and SYCP1 for homolog synapsis (de Vries et al., 2005). Although γH2AX signals were detected (Figure 4A), DMC1 foci were rarely observed in the *Meiosin* KO preleptotene-like cells (Figures 4B and 4C). Accordingly, SYCP1 was not observed in the *Meiosin* KO preleptotene-like cells (Figures 4D and 4E). These indicated that *Meiosin* KO spermatocyte-like cells failed to undergo meiotic recombination and homolog synapsis, supporting the notion that progression of meiotic prophase I was aborted in *Meiosin* KO.

Consistent with the previous report on *Stra8* KO testis (Mark et al., 2008), some fraction, if not all, of SYCP3+ cells in *Stra8* KO testis showed more advanced stage markers, DMC1 and SYCP1 with more extended SYCP3-stained axes (Figures 4A–4E), albeit elongation was partial compared to WT. This indicates that preleptotene block was more severe in *Meiosin* KO than *Stra8* KO. It is possible that this difference was due to the mixed genetic background of our *Stra8* KO, which shows milder effect on meiotic initiation compared to C57BL/6 background (Anderson et al., 2008).

Transcriptome analysis on the entire testis was performed to address whether the observed phenotype in *Meiosin* KO testes accompanied alteration in gene expression. Although the cellular composition of testes changes during development, we assumed the first wave of spermatocyte should progress with same cellular composition in WT, *Meiosin* KO, and *Stra8* KO juvenile testes until the defects appear in the mutants. Principal component analysis (PCA) revealed that the overall transcriptomes of the *Meiosin* KO and *Stra8* KO testis were different from those of the WT testes during P10–P21 (period of the initial wave of spermatocyte progression, which starts from the meiotic entry until the completion of meiotic prophase) (Figure 4F; Table S1), but rather close to that of P8 WT testis, where most of the cells are yet to reach meiotic initiation. Notably, gene ontology (GO) analysis of differentially expressed genes (DEG) between P10 WT (when the initial wave starts at the meiotic entry) and *Meiosin* KO testes indicated that reproduction-associated genes including those involved in the processes of meiotic chromosomes, meiotic cell cycle, and spermatogenesis were downregulated in *Meiosin* KO testes (Figures 4G and S4A; Table S2).

We noticed that a subset of meiotic genes was more downregulated in *Meiosin* KO compared to *Stra8* KO (Figures 4H and S4B; Table S3), which may account for the aforementioned cytological observation that preleptotene block was more severe in *Meiosin* KO than *Stra8* KO (Figures 4B–4E).

To further confirm the assumption above, we examined preleptotene-enriched population to analyze the transcriptomes at the time of meiotic entry. The preleptotene-enriched population was isolated from WT and *Meiosin* KO testes on the *Stra8-3FH-p2A-GFP* KI background by fluorescent sorting of GFP positive cells (Figure S5A). Because the number of GFP positive cells from *Meiosin* KO testes was limited, we analyzed the transcriptomes of STRA8 expressing cells using SMART-seq that allows the analysis with small cell number (Figure S5; Table S4). PCA indicated that the overall transcriptomes in the STRA8 (GFP) positive cells were different between WT and *Meiosin* KO (Figure S5B). GO analysis of DEGs in preleptotene-enriched populations suggested that expression levels of male reproduction-associated genes were downregulated in *Meiosin* KO (Figures S5D and S5E; Table S4). These findings were consistent with the cytological observation that *Meiosin* KO spermatocyte-like cells failed to progress into meiosis and spermatogenesis. Thus, these results suggest that MEIOSIN, in collaboration with STRA8, is required for meiotic prophase program in male.

MEIOSIN Plays a Critical Role in Meiotic Entry Decision under RA Signaling during Spermatogenesis

RA and the RA receptors (RARs) play pivotal roles in germ cell differentiation and meiotic initiation during spermatogenesis (Anderson et al., 2008; van Pelt and de Rooij, 1991). During spermatogenesis, the first expression of *Stra8* occurs in differentiating spermatogonia, and then the second expression occurs in preleptotene spermatocytes in response to RA (Mark et al., 2008; Endo et al., 2015; Zhou et al., 2008). To date, no clear explanation has been provided why meiosis is initiated only after the second RA-dependent induction of STRA8, despite its expression in both cell populations.

Therefore, we investigated the role of RA signaling in the regulation of MEIOSIN expression during spermatogenesis. The initial wave of spermatogonial differentiation and meiotic initiation occurs in testes around P2–P3 and P9–P10, respectively (Busada et al., 2014; Drumond et al., 2011). The RA synthesis inhibitor WIN 18,446 is known to suppress spermatogonial differentiation and meiotic initiation (Amory et al., 2011; Endo et al., 2015; Hogarth et al., 2011; Evans et al., 2014). Consecutive injection of WIN 18,446 in neonatal male mice between P5 to P11 repressed the expression of both STRA8 and MEIOSIN, whereas administration of RA one day after the final injection induced the expression of STRA8 and MEIOSIN in WIN 18,446-treated testes (Figure 5A). MEIOSIN expression is independent of STRA8 (Figure 2G). Thus, like STRA8, MEIOSIN may be induced directly in response to RA.

To examine this possibility, we utilized germline stem (GS) cells (Kanatsu-Shinohara et al., 2003) that are established from spermatogonial stem cells and can enter meiotic prophase by the treatment with RA *in vitro*. Indeed, in GS cells, RARs bound to the promoter regions of the *Meiosin* and *Stra8* loci to enable RA-dependent expressions, which accompanied H3 lysine27 acetylation (H3K27ac), a marker of active chromatin state (Figures 5B and 5C). The induction of *Meiosin* by RA was slower than that of *Stra8* in GS cells, which may reflect the earlier *in vivo* activation of *Stra8* (Mark et al., 2008; Endo et al., 2015; Zhou et al., 2008).

Interestingly, the expression of MEIOSIN was restricted to preleptotene spermatocytes, although STRA8 was induced in both spermatogonia (marked by PLZF) and preleptotene spermatocytes in response to RA (Figure 5D). Notably, it has been proposed that DMRT1 prevents premature meiotic entry in spermatogonia by repressing RA-dependent transcription (Matson et al., 2010). Immunostaining analysis indicated that DMRT1 and MEIOSIN exhibited a mutually exclusive expression in the testis (Figure 5E). Moreover, our reanalysis of the previous

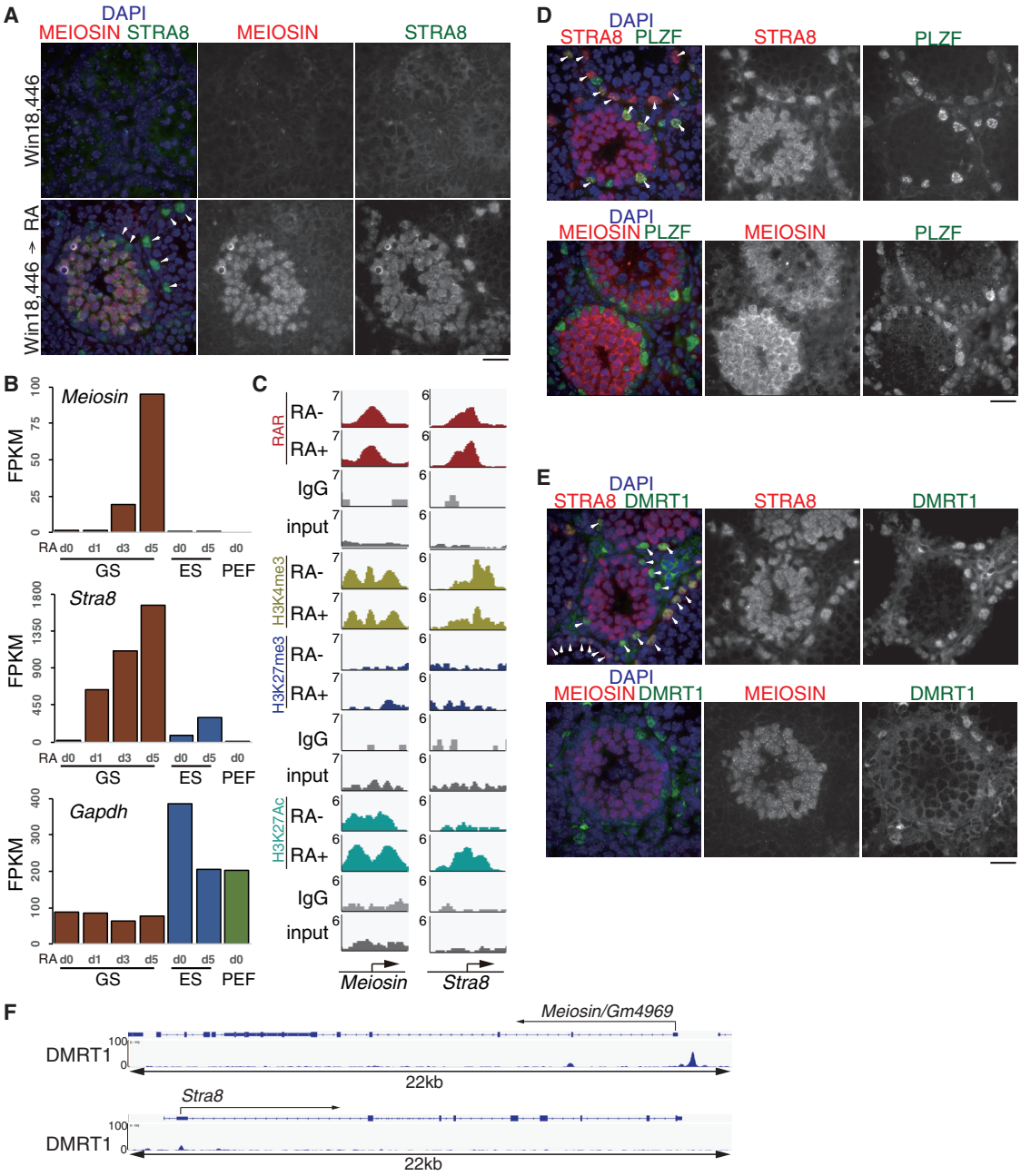

Figure 5. MEIOSIN Is Critical for Meiotic Entry Decision under RA Signaling during Spermatogenesis

(A) WT neonatal male mice were subjected to consecutive injection of a RA synthesis inhibitor WIN 18,446 from P5 to P11, followed by RA or carrier injection at P12. Seminiferous tubule sections at P13 were stained for MEIOSIN, STRA8, and DAPI. White arrowheads: STRA8+/MEIOSIN-negative spermatogonia. Note that the expressions of both STRA8 and MEIOSIN were repressed after WIN 18,446 treatment and restored after RA injection.

(B) The expression levels of *Meiosin* (upper), *Stra8* (middle), and *Gapdh* (lower) were analyzed using RNA-seq. FPKM: fragments per kilobase of exon per million mapped reads. GS cells and embryonic stem (ES) cells were exposed to RA for 0–5 days. PEF: primary embryonic fibroblast. Note that GS cells showed the expressions of *Meiosin* and *Stra8* in response to RA, whereas ES cells showed the expression of *Stra8* but not *Meiosin*.

(C) Chromatin binding levels of RA receptor (pan-RAR), H3K4me3, H3K27me3, and H3K27ac in GS cells with or without RA treatment were analyzed by ChIP-seq analysis. Of note, the RAR bound to the promoter regions of *Meiosin* and *Stra8* in GS cells. Data represent fold enrichment calculated using local lambda values. Control IgGs and input DNA reads (RA-) are also shown. Details of the transcriptome and ChIP-seq analyses in GS cells are deposited in the GEO (GSE116798).

(D) Seminiferous tubule sections treated as in (A) were stained for STRA8 (upper) or MEIOSIN (lower), with PLZF and DAPI. White arrowheads: STRA8+/ PLZF+ spermatogonia. Note that MEIOSIN was detected both in the nuclei and the cytoplasm one day after administration of RA, whereas MEIOSIN was mostly localized in the nuclei in stage VII/VIII tubules in physiological condition.

(E) Seminiferous tubule sections were stained for STRA8 (upper) or MEIOSIN (lower), with DMRT1 and DAPI as in (A). White arrowheads: STRA8+/DMRT+ spermatogonia.

(F) Genomic view of DMRT1 binding to *Meiosin* and *Stra8* loci, obtained from the previous DMRT1 ChIP-seq data (Murphy et al., 2015). Scale bars: 25 μm.

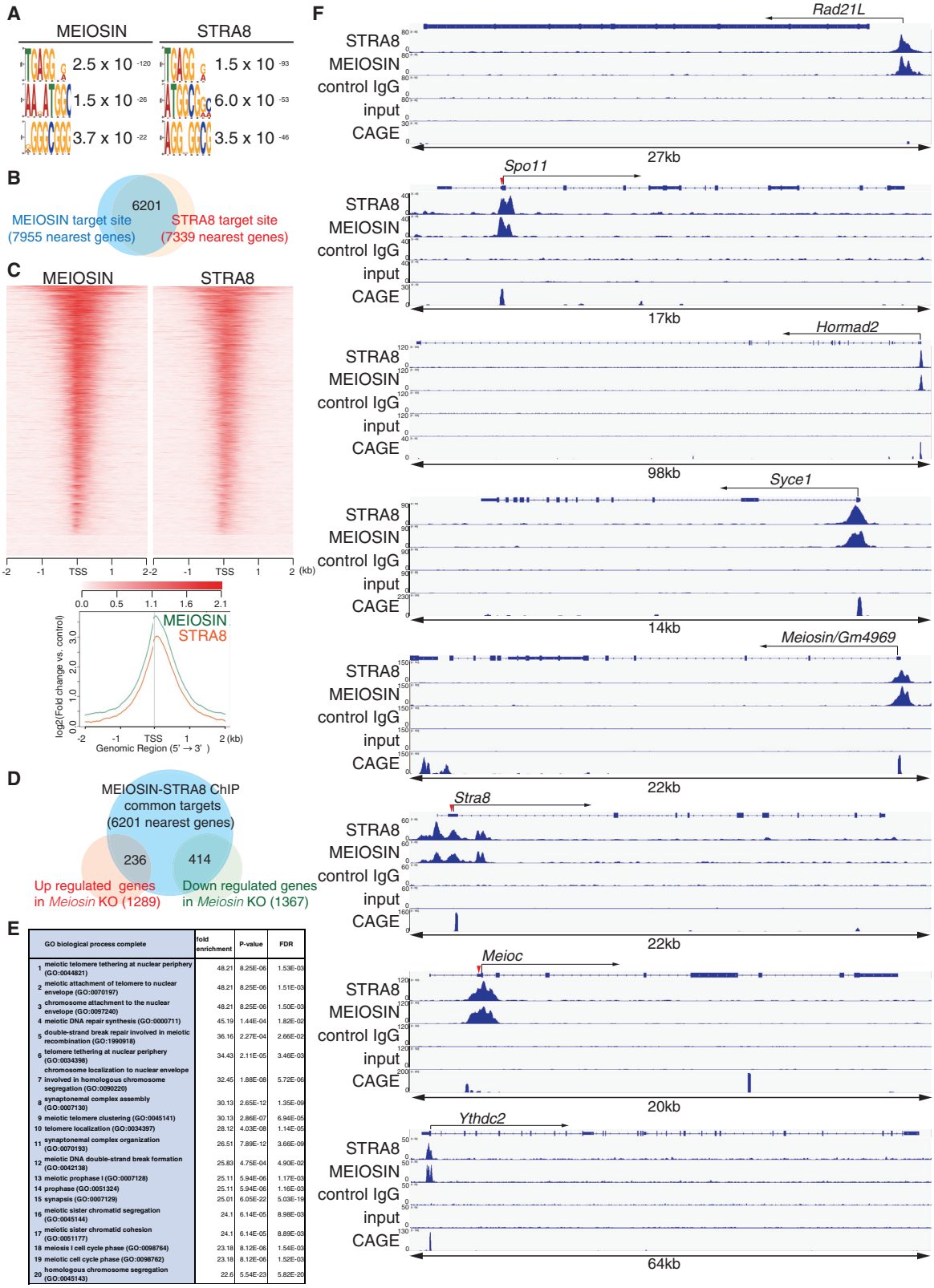

	GO biological process complete	fold enrichment	P-value	FDR
1	meiotic telomere tethering at nuclear periphery (GO:0044821)	48.21	8.25E-06	1.53E-03
2	meiotic attachment of telomere to nuclear envelope (GO:0070197)	48.21	8.25E-06	1.51E-03
3	chromosome attachment to the nuclear envelope (GO:0097240)	48.21	8.25E-06	1.50E-03
4	meiotic DNA repair synthesis (GO:0000711)	45.19	1.44E-04	1.82E-02
5	double-strand break repair involved in meiotic recombination (GO:1990918)	36.16	2.27E-04	2.66E-02
6	telomere tethering at nuclear periphery (GO:0034398)	34.43	2.11E-05	3.46E-03
7	chromosome localization to nuclear envelope involved in homologous chromosome segregation (GO:0090220)	32.45	1.88E-08	5.72E-06
8	synaptonemal complex assembly (GO:0007130)	30.13	2.65E-12	1.35E-09
9	meiotic telomere clustering (GO:0045141)	30.13	2.86E-07	6.94E-05
10	telomere localization (GO:0034397)	28.12	4.03E-08	1.14E-05
11	synaptonemal complex organization (GO:0070193)	26.51	7.89E-12	3.66E-09
12	meiotic DNA double-strand break formation (GO:0042138)	25.83	4.75E-04	4.90E-02
13	meiotic prophase I (GO:0007128)	25.11	5.94E-06	1.17E-03
14	prophase (GO:0051324)	25.11	5.94E-06	1.16E-03
15	synapsis (GO:0007129)	25.01	6.05E-22	5.03E-19
16	meiotic sister chromatid segregation (GO:0045144)	24.1	6.14E-05	8.98E-03
17	meiotic sister chromatid cohesion (GO:0051177)	24.1	6.14E-05	8.89E-03
18	meiosis I cell cycle phase (GO:0098764)	23.18	8.12E-06	1.54E-03
19	meiotic cell cycle phase (GO:0098762)	23.18	8.12E-06	1.52E-03
20	homologous chromosome segregation (GO:0045143)	22.6	5.54E-23	5.82E-20

Figure 6. MEIOSIN and STRA8 Bind to the Meiotic Gene Promoters

(A) Top 3 ranked sequence motifs enriched in MEIOSIN ChIP-seq (left) and STRA8 ChIP-seq (right) with E values.

(B) Venn diagram representing the overlap of MEIOSIN-target sites (7,955 nearest genes) and STRA8- target sites (7,339 nearest genes).

(legend continued on next page)

DMRT1 ChIP-seq data (Murphy et al., 2015) showed its binding to the 5′ upstream of *Meiosin* locus, suggesting that DMRT1 may repress *Meiosin* expression in spermatogonia (Figure 5F). This accounts for why RA does not induce MEIOSIN expression and meiosis in differentiating spermatogonia. We noticed that STRA8 and DMRT1 were coexpressed in some, if not all, spermatogonia (Figure 5E). Since DMRT1 ChIP-seq showed a marginal binding peak at *Stra8* locus (Figure 5F), repression of *Stra8* by DMRT1 in spermatogonia could be less strict compared to that of *Meiosin*. This indicates *Stra8* expression alone is not sufficient for the induction of meiosis in spermatogonia. Thus, it is reasonable to assume that STRA8+ cells undergo meiosis during spermatogenesis exclusively when MEIOSIN and STRA8 are coexpressed. Therefore, MEIOSIN together with STRA8 determines meiotic entry decision in response to RA during spermatogenesis.

MEIOSIN and STRA8 Bind and Activate a Subset of Meiotic Prophase Genes

MEIOSIN possesses putative DNA-binding domains (Figure 1C) and might act in a transcriptional complex that contains STRA8. Therefore, MEIOSIN- and STRA8-target sites on the genome were further investigated with chromatin IP followed by sequencing (ChIP-seq) analysis using testes. The results of this analysis showed that MEIOSIN bound to 9,876 sites, of which 28.0% and 23.6% resided within 500 bp of promotor regions and in the 5′ UTR on the mouse genome, respectively (Figures S6A–S6C). Remarkably, GO analysis of MEIOSIN-ChIP targets (7,955 nearest genes, which were assigned regardless of the distance from the MEIOSIN-binding sites) revealed that genes assigned to meiotic processes and also to the processes not restricted to meiosis (such as histone modification and chromatin regulation) were enriched (Figure S6D; Table S5). Among the MEIOSIN-bound genes, 1,085 genes were commonly identified with downregulated genes in *Meiosin* KO GFP positive cells, whose functions were associated with meiosis or reproduction (Figure S5F). STRA8 ChIP-seq analysis showed that STRA8 bound to 8,801 sites, of which 24.7% and 24.6% resided within 500 bp of promotor regions and in the 5′ UTR, respectively (Figure S6E). Similar to the MEIOSIN targets, GO analysis of STRA8-ChIP targets (7,339 nearest genes) revealed enrichment of the genes for meiosis-specific processes and also those that are not restricted to meiosis (Figure S6F; Table S5). This trend was consistent with STRA8-FLAG ChIP-seq data in the previous study (Kojima et al., 2019) (Figure S6G).

Notably, MEIOSIN- and STRA8-ChIP enriched one shared motif out of the top 3 DNA-binding motifs (Figure 6A). Accordingly, MEIOSIN and STRA8 commonly bound to 6,201 genes (overlap of the genes possessing common peaks) (Figures 6B and S6H; Table S5). Most of the MEIOSIN- and STRA8-binding sites resided within ± 2 kb of the transcription strat site (TSS) rather than the upstream regions (Figure 6C). Crucially, MEIOSIN- and STRA8-binding sites well overlapped at the 5′-capped sequence of mRNA, which were revealed by Cap analysis gene expression (CAGE)-seq in P10.5 testis (Li et al., 2013) (Figure 6F). Among the MEIOSIN- and STRA8-bound genes, 414 genes were commonly identified with those downregulated in *Meiosin* KO testes (Figure 6D; Table S5), whose functions were associated with meiosis (Figure 6E). These include genes essential for meiotic chromosome dynamics and recombination (Figure 6F), suggesting that the MEIOSIN-STRA8 complex directly activates the transcription of a subset of critical meiotic genes. For example, RAD21L (Ishiguro et al., 2014; Lee and Hirano, 2011; Llano et al., 2012) is a meiosis-specific cohesin subunit. SYCP2 (Yang et al., 2006), SYCE1 (Costa et al., 2005), SYCE2 (Bolcun-Filas et al., 2007), SYCE3 (Schramm et al., 2011), and TEX12 (Hamer et al., 2006) constitute the structural components of the synaptonemal complex. HORMAD1 and HORMAD2 monitor homolog synapsis (Wojtasz et al., 2012). Meiosis-specific telomere proteins MAJIN (Shibuya et al., 2015) and TERB1 (Shibuya et al., 2014) drive chromosome movement in homolog synapsis. SPO11 (Baudat et al., 2000; Romanienko and Camerini-Otero, 2000), DMC1 (Pittman et al., 1998; Yoshida et al., 1998), PRDM9 (Baudat et al., 2010), TOP6BL/Gm960 (Robert et al., 2016; Vrielynck et al., 2016), and MSH5 (de Vries et al., 1999) are involved in meiotic recombination. Thus, MEIOSIN and STRA8 promote the transcription of genes essential for meiotic chromosome dynamics.

Notably, MEIOSIN and STRA8 bound to their own promoter regions (Figure 6F), suggesting autoactivation feedback loop, which ensures rapid expression during the short period of meiotic initiation. Interestingly, MEIOSIN and STRA8 also bound to the promoter regions of the *Meioc* and *Ythdc2* genes (Figure 6F), whose products destabilize mitotic cell-cycle-associated transcripts (Abby et al., 2016; Soh et al., 2017). In the *Meioc* KO and *Ythdc2* KO mice, germ cells initiate but fail to maintain the meiotic prophase, showing misexpression of mitotic cyclin A2 and metaphase-like chromosome condensation (Soh et al., 2017; Jain et al., 2018). This mitotic status is also observed in *Meiosin* KO and *Stra8* KO mice (Figure 3; Table S4). Therefore, the cell-cycle-switching program from mitosis to meiosis might be mediated via the MEIOSIN-STRA8 complex through, at least in part, the activation of *Meioc* and *Ythdc2* transcription. These findings suggest that the MEIOSIN-STRA8 complex binds and activates a subset of meiotic genes.

(C) Heatmap of the common binding sites (6,201 genes) of MEIOSIN and STRA8 at the positions −2.0 kb upstream to +2.0 kb downstream relative to the TSS. Color key is shown. Average distribution of MEIOSIN- and STRA8-binding peak (lower).

(D) Venn diagram representing the overlap of common MEIOSIN and STRA8 targets (6,201 genes), downregulated (1,367 genes), and upregulated (1,289 genes) genes in *Meiosin* KO mice.

(E) GO analysis of the biological functions of MEIOSIN- and STRA8-bound genes that were downregulated in *Meiosin* KO mice (414 genes) indicated that meiotic genes were enriched over 22,296 mouse reference genes. Those of MEIOSIN- and STRA8-bound genes that were upregulated in *Meiosin* KO mice (236 genes) are shown in Table S5.

(F) Genomic view of MEIOSIN (rep.1), STRA8, and control IgG ChIP-seq, input DNA data over representative commonly bound meiotic gene loci (*Rad21L, Spo11*, *Hormad2*, *Syce1*, *Meiosin/Gm4969*, *Stra8*, *Meioc,* and *Ythdc2*). To specify testis specific TSS, RNA-seq of the 5′ capped end of the mRNA (CAGE) in P10.5 testis is shown (Li et al., 2013). Genomic coordinates were obtained from Ensembl. Red arrowheads in *Spo11*, *Stra8*, and *Meioc* indicate putative first exon annotated in RefSeq.

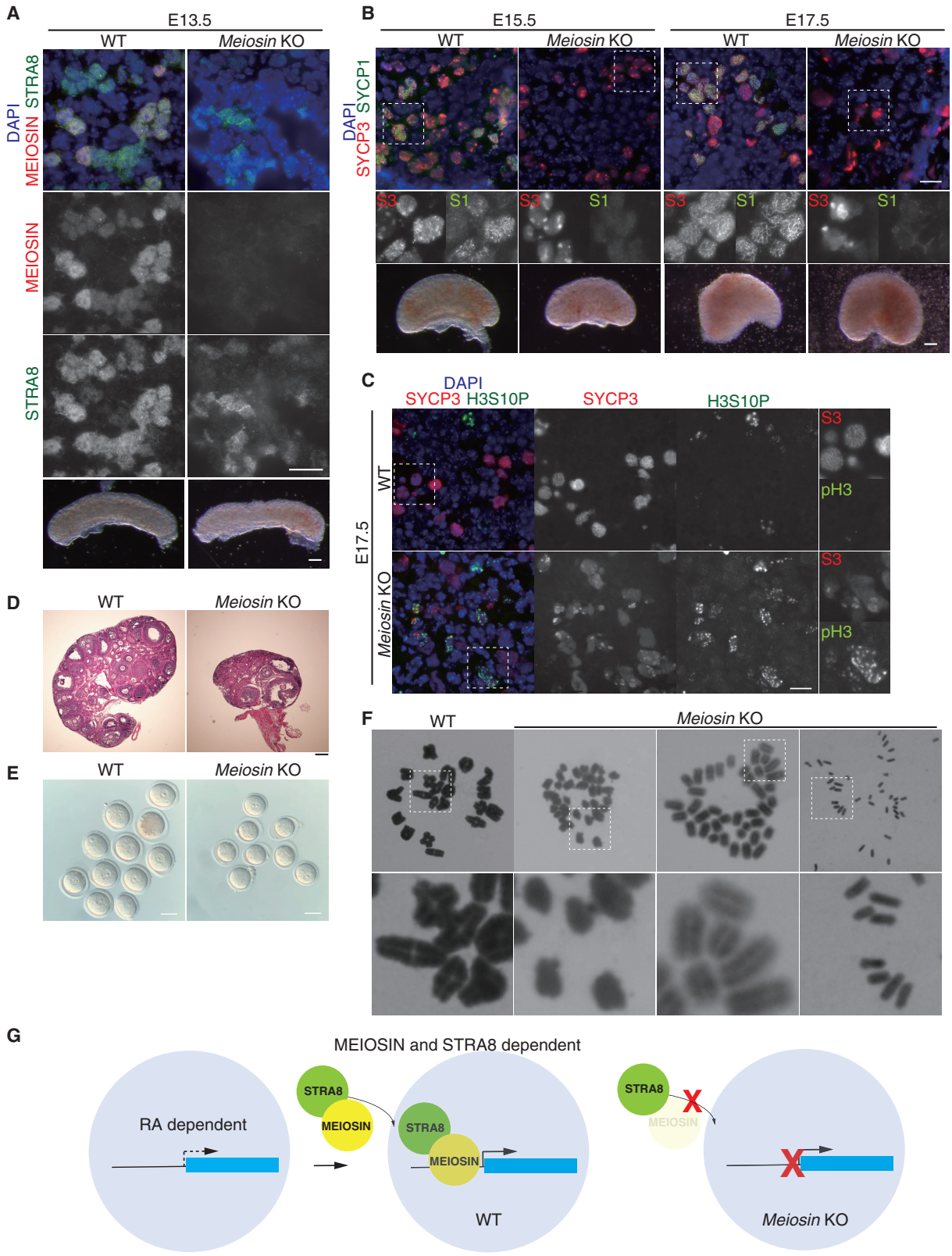

Figure 7. Initiation of Meiosis Is Defective in *Meiosin* KO Ovaries

(A) Embryonic ovary sections (E13.5) from WT and *Meiosin* KO were stained for MEIOSIN, STRA8, and DAPI. Scale bar: 25 μm. Isolated ovaries are shown on the bottom. Scale bar: 100 μm. (B) Embryonic ovary sections (E15.5, E17.5) from WT and *Meiosin* KO were stained for SYCP3, SYCP1, and DAPI. Scale bar: 25 μm.

(legend continued on next page)

MEIOSIN Is Required for Meiotic Initiation in Female

In *Meiosin* KO ovaries, STRA8 was expressed at E13.5 (Figure 7A). *Meiosin* KO ovarian germ cells persistently showed patchy aggregates of SYCP3 during E13.5–E17.5 and failed to undergo homolog synapsis (Figure 7B), though no morphological difference in ovaries was observed compared to WT. Furthermore, a subpopulation of SYCP3+ germ cells in *Meiosin* KO ovary at E17.5 showed premature H3S10P on chromatin. These observations suggested that *Meiosin* KO ovarian germ cells underwent mitotic status rather than meiotic prophase as has been observed in *Meiosin* KO testes (Figures 3A–3D).

Histological analysis revealed that ovaries were degenerated with apparently fewer mature follicles at the age of 4 weeks old in *Meiosin* KO (Figure 7D), suggesting that ovarian germ cell loss was accelerated in *Meiosin* KO. Notably, despite the defective meiotic prophase, we noticed that a small population of *Meiosin* KO ovarian germ cells survived and differentiated into oocyte-like cells. To examine the cellular morphology, we isolated oocyte-like cells from *Meiosin* KO ovaries (4 weeks old) after hormonal injection (Figure 7E). *Meiosin* KO oocyte-like cells exhibited germinal vesicles (GV) and zona pellucida, which were apparently the same morphology as WT GV oocytes. We next examined the chromosome morphologies of *Meiosin* KO oocytes-like cells 5–6 h after GV break down (GVBD), when WT chromosomes would undergo condensation before the first meiotic division. Giemsa staining of the chromosomes revealed that 20 pairs of bivalents with chiasma were observed in WT oocytes (Figure 7F). Crucially, in contrast, 40 univalents (sister chromatids) or 40 single chromatids were observed in *Meiosin* KO oocytes-like cells (Figure 7F). This observation suggested that some population of *Meiosin* KO ovarian germ cells failed to undergo DNA replication during fetal period. Moreover, lack of chiasma indicated that *Meiosin* KO ovarian germ cells failed to undergo meiotic recombination (Figure 7F), corroborating our observation that *Meiosin* KO oocyte-like cells may have skipped the meiotic prophase (Figure 7B). Collectively, these data indicate that MEIOSIN plays a crucial role in cell-cycle switching from mitosis to meiosis in female. This observation is consistent with the previous study showing that oocyte-like cells were produced without entering meiosis in *Stra8* KO mice (Dokshin et al., 2013). Therefore, one important implication is that the meiotic cell cycle directed by the MEIOSIN-STRA8 complex is a genetically separable program from the differentiation of ovarian germ cell.

DISCUSSION

Meiotic prophase I is a specialized stage that is equivalent to prolonged G2 phase of the cell cycle during which meiosis-specific chromosome events such as AE formation, meiotic recombination, and homolog synapsis sequentially occur (Baudat et al., 2013; Cahoon and Hawley, 2016; Handel and Schimenti, 2010; Page and Hawley, 2004; Zickler and Kleckner, 2015). Previously, it was shown that STRA8 binds and activates promoters of germline-specific genes for meiosis and those of G1-S cell-cycle regulation (Kojima et al., 2019). In this study, we demonstrate that not only STRA8 but also MEIOSIN is required for the initiation of meiosis. We have shown that MEIOSIN and STRA8 bind and activate a substantial number of meiotic genes that are essential for establishing meiosis-specific chromosome structure. It should be mentioned that MEIOSIN and STRA8 also bind to the genes that are related to repressive histone modification and chromatin silencing, such as Histone methyl transferases and the components of polycomb repressive complex (Figure S6H; Table S5). This suggests that MEIOSIN and STRA8 may also play a role in suppressing soma-specific transcription through those chromatin repressive factors as suggested by previous study (Mu et al., 2014). Furthermore, MEIOSIN and STRA8 bind and activate *Meioc* and *Ythdc2* genes (Figure 6F), whose products prevent mitotic cell-cycle-associated transcripts from translation (Abby et al., 2016; Soh et al., 2017; Jain et al., 2018). Thus, MEIOSIN together with STRA8 plays crucial roles in suppressing mitotic program and coordinating the cell cycle with meiotic prophase-specific chromosome events. Therefore, MEIOSIN together with STRA8 acts as an upstream regulator for cell-cycle switching from mitosis to meiosis, rather than one of the factors maintaining meiotic prophase.

Because STRA8 is expressed in differentiating spermatogonia as well as preleptotene spermatocytes (Figure 5), we cannot officially exclude the possibility that a subset of our STRA8 ChIP-seq binding sites might derive from the minor population of differentiating spermatogonia. Since defect in spermatogonial differentiation was evident in aged *Stra8* KO testes on C57BL/6 background (Endo et al., 2015), STRA8 alone may have other specific role in the transcription that are not restricted to meiosis in differentiating spermatogonia.

Our ChIP-seq analyses indicate that MEIOSIN and STRA8 overall bind to the TSSs rather than upstream promoters or enhancer regions (Figure 6C). Given that meiotic gene promoters are often poised by enrichment of H3K4me2 and loading of RNA polymerase II in spermatogonia (Sin et al., 2015), MEIOSIN and STRA8 may promote the release of paused RNA polymerase II at the target TSSs (Williams et al., 2015) for a rapid and synchronous burst of their transcription.

Our study demonstrated that coexpression of MEIOSIN and STRA8 is crucial for decision of meiotic entry under RA. However, ectopic expression of MEIOSIN and STRA8 was not sufficient to induce meiosis in *in-vitro*-cultured cells (data not shown).

Enlarged images are shown (S1: SYCP1, S3: SYCP3). Isolated ovaries are shown on the bottom. Scale bar: 100 μm. Note that WT oocytes underwent homolog synapsis by E15.5, while no oocytes later than preleptotene-like stage appeared in *Meiosin* KO.

(C) Embryonic ovary Sections (E17.5) from WT and *Meiosin* KO were stained for SYCP3, H3S10P, and DAPI. Enlarged images are shown on the right. Scale bar: 25 μm.

(D) Hematoxylin and eosin staining of the sections from WT and *Meiosin* KO ovaries (4-week-old). Scale bar: 200 μm.

(E) GV oocytes isolated from WT (left) and oocyte-like cells isolated from *Meiosin* KO (right). Scale bars: 50 μm.

(F) Giemsa staining of metaphase I bivalents in WT (most left), metaphase-like univalent (middle left and right), and single chromatids (most right) in *Meiosin* KO oocyte-like cells. Enlarged images are shown on the bottom.

(G) Schematic illustrations of sequential activation by RA dependent- followed by the MEIOSIN-STRA8 complex dependent process on a subset of meiotic prophase genes in WT and *Meiosin* KO.

It is possible that epigenetic restriction such as DNA methylation (Yamaguchi et al., 2012) and PRC-mediated repression (Yokobayashi et al., 2013; Endoh et al., 2017) is imposed to meiotic genes prior to initiation of meiosis. In mitotic cells, meiotic genes are suppressed by MAX (Suzuki et al., 2016) and E2F-6 (Pohlers et al., 2005; Kehoe et al., 2008; Leseva et al., 2013). Thus, multiple repressive mechanisms act on meiotic genes. It is known that RA also activates some set of meiotic genes in a STRA8-independent manner (Koubova et al., 2014; Soh et al., 2015). Furthermore, it has been shown that RA and STRA8 are not sufficient for female germ cell differentiation of primordial germ cell (PGC)-like cells, and that BMP and RA synergistically contribute to meiotic entry (Miyauchi et al., 2017). Therefore, it is possible that multiple layer of regulation potentiates the competency for meiotic gene activation prior to the action of the MEIOSIN-STRA8 complex (Figure 7G), and the MEIOSIN-STRA8 complex may be at the upstream of robust transcriptional activation to amplify meiotic transcripts at the mitosis to meiosis transition.

It has been proposed that STRA8 possesses a putative bHLH (Baltus et al., 2006; Tedesco et al., 2009) and HMG domain (Kojima et al., 2019). Similarly, MEIOSIN possesses bHLH and HMG DNA-binding domains (Figure 1C). It is possible that the interplay between MEIOSIN and STRA8 might be mediated through those domains that provide binding specificity to the meiotic promoter regions. Furthermore, MEIOSIN plays a central role in meiotic entry decision under RA signaling, when it is coexpressed with STRA8 (Figure 5). Overall, it is suggested that MEIOSIN and STRA8 act in the same transcriptional complex for the initiation of meiosis, both in male and female (Figure 7G).

The meiotic developmental program has been studied in budding yeast and fission yeast. In both types of yeast, external environmental signals converge for transcriptional and posttranscriptional regulation of the master regulators, IME1 and Ste11 in budding and fission yeast, respectively (van Werven and Amon, 2011; Sugimoto et al., 1991). As there is no significant structural homology among the regulators including STRA8, evolutionary conservation of the meiotic entry system has remained controversial (van Werven and Amon, 2011; Anandhakumar et al., 2013). Intriguingly, similar to MEIOSIN and STRA8, Ste11 possesses an HMG-box that recognizes specific DNA sequences located in the promoters of the reproduction-related genes (Sugimoto et al., 1991). Moreover, many of HMG-box proteins are central to the control of sexual differentiation in the ascomycetes (Nelson, 1996). Thus, our study will shed light on the evolutionally conserved mechanism of cell-cycle switching from mitosis to meiosis in eukaryotes.

STAR★METHODS

Detailed methods are provided in the online version of this paper and include the following:

SUPPLEMENTAL INFORMATION

Supplemental Information can be found online at https://doi.org/10.1016/j.devcel.2020.01.010.

ACKNOWLEDGMENTS

The authors thank Takashi Seki (Liaison Laboratory Research Promotion Center, IMEG, Kumamoto University), Etsushi Kitamura, and Hiromi Kimura for technical support, and Minetaro Ogawa, Masatake Araki, and Narumi Koga for provision of materials. GS (DBA/2) and ES (KY1.1) cell lines were kindly provided by Drs. Takashi Shinohara and Junji Takeda, respectively. The authors also thank Drs. Marry Ann Handel, David Page, Shosei Yoshida, Kodai Hirano, Yumiko Saga, Akira Nakamura, Tsutomu Endo, Yoshinori Watanabe, and Satoshi Namekawa for their valuable discussion. This work was supported in part by KAKENHI grant #19H05748 (to H.N.), KAKENHI grant #16H01257, #16H01221, #17H03634, #18K19304, #19H05245, #19H05743, and #JP 16H06276 from MEXT, Japan; NIG-JOINT (44A2017, 40A2018, and 32A2019); the program of the Joint Usage/ IMEG Research Center for Developmental Medicine; Takeda Science Foundation; Yamada Science Foundation; Ichiro Kanehara Foundation for Medical Science and Medical Care (to K.I.).

AUTHOR CONTRIBUTIONS

K.I. conducted the study, performed most of the experiments in mice, and wrote the manuscript. N. Takeda, M.S., and K.A. generated *Stra8-3FH-GFP* KI mouse, *Meiosin* KO, and *Stra8* KO mice. N. Tani performed the mass spectrometry analysis. K.M. and H.N. performed the MEIOSIN and STRA8 ChIP-seq analysis in mouse testes. S.U. and M.Y. performed the RNA-seq and SMART-seq analysis. M.H. and S.C. performed the ChIP-seq and RNA-seq in GS cells. H.N. conducted the homolog search. M.S.H.K. supported the study. M.S. and K.I. performed embryonic gonad experiments. N. Takeda and K.I. performed GV oocyte experiments. S.F. performed histological analysis. The experimental design and interpretation of data were conducted by K.I., K.A., and H.N.

DECLARATION OF INTERESTS

The authors declare no competing interests.

Received: July 17, 2019
Revised: October 10, 2019
Accepted: January 9, 2020
Published: February 6, 2020

REFERENCES

Abby, E., Tourpin, S., Ribeiro, J., Daniel, K., Messiaen, S., Moison, D., Guerquin, J., Gaillard, J.C., Armengaud, J., Langa, F., et al. (2016). Implementation of meiosis prophase I programme requires a conserved retinoid-independent stabilizer of meiotic transcripts. Nat. Commun. *7*, 10324.

Amano, T., Hirata, T., Falco, G., Monti, M., Sharova, L.V., Amano, M., Sheer, S., Hoang, H.G., Piao, Y., Stagg, C.A., et al. (2013). Zscan4 restores the developmental potency of embryonic stem cells. Nat. Commun. *4*, 1966.

Amory, J.K., Muller, C.H., Shimshoni, J.A., Isoherranen, N., Paik, J., Moreb, J.S., Amory, D.W., Sr., Evanoff, R., Goldstein, A.S., and Griswold, M.D. (2011). Suppression of spermatogenesis by bisdichloroacetyldiamines is mediated by inhibition of testicular retinoic acid biosynthesis. J. Androl. *32*, 111–119.

Anandhakumar, J., Fauquenoy, S., Materne, P., Migeot, V., and Hermand, D. (2013). Regulation of entry into gametogenesis by Ste11: the endless game. Biochem. Soc. Trans. *41*, 1673–1678.

Anderson, E.L., Baltus, A.E., Roepers-Gajadien, H.L., Hassold, T.J., de Rooij, D.G., van Pelt, A.M., and Page, D.C. (2008). Stra8 and its inducer, retinoic acid, regulate meiotic initiation in both spermatogenesis and oogenesis in mice. Proc. Natl. Acad. Sci. USA *105*, 14976–14980.

Bailey, T.L. (2011). DREME: motif discovery in transcription factor ChIP-seq data. Bioinformatics *27*, 1653–1659.

Baltus, A.E., Menke, D.B., Hu, Y.C., Goodheart, M.L., Carpenter, A.E., de Rooij, D.G., and Page, D.C. (2006). In germ cells of mouse embryonic ovaries, the decision to enter meiosis precedes premeiotic DNA replication. Nat. Genet. *38*, 1430–1434.

Baudat, F., Buard, J., Grey, C., Fledel-Alon, A., Ober, C., Przeworski, M., Coop, G., and de Massy, B. (2010). PRDM9 is a major determinant of meiotic recombination hotspots in humans and mice. Science *327*, 836–840.

Baudat, F., Imai, Y., and de Massy, B. (2013). Meiotic recombination in mammals: localization and regulation. Nat. Rev. Genet. *14*, 794–806.

Baudat, F., Manova, K., Yuen, J.P., Jasin, M., and Keeney, S. (2000). Chromosome synapsis defects and sexually dimorphic meiotic progression in mice lacking Spo11. Mol. Cell *6*, 989–998.

Bolcun-Filas, E., Costa, Y., Speed, R., Taggart, M., Benavente, R., De Rooij, D.G., and Cooke, H.J. (2007). SYCE2 is required for synaptonemal complex assembly, double strand break repair, and homologous recombination. J. Cell Biol. *176*, 741–747.

Bowles, J., Knight, D., Smith, C., Wilhelm, D., Richman, J., Mamiya, S., Yashiro, K., Chawengsaksophak, K., Wilson, M.J., Rossant, J., et al. (2006). Retinoid signaling determines germ cell fate in mice. Science *312*, 596–600.

Busada, J.T., Kaye, E.P., Renegar, R.H., and Geyer, C.B. (2014). Retinoic acid induces multiple hallmarks of the prospermatogonia-to-spermatogonia transition in the neonatal mouse. Biol. Reprod. *90*, 64.

Cahoon, C.K., and Hawley, R.S. (2016). Regulating the construction and demolition of the synaptonemal complex. Nat. Struct. Mol. Biol. *23*, 369–377.

Costa, Y., Speed, R., Ollinger, R., Alsheimer, M., Semple, C.A., Gautier, P., Maratou, K., Novak, I., Höög, C., Benavente, R., et al. (2005). Two Novel Proteins Recruited by Synaptonemal Complex Protein 1 (SYCP1) are at the centre of meiosis. J. Cell Sci. *118*, 2755–2762.

de Vries, F.A., de Boer, E., van den Bosch, M., Baarends, W.M., Ooms, M., Yuan, L., Liu, J.G., van Zeeland, A.A., Heyting, C., and Pastink, A. (2005). Mouse Sycp1 functions in synaptonemal complex assembly, meiotic recombination, and XY body formation. Genes Dev. *19*, 1376–1389.

de Vries, S.S., Baart, E.B., Dekker, M., Siezen, A., de Rooij, D.G., de Boer, P., and te Riele, H. (1999). Mouse MutS-like protein Msh5 is required for proper chromosome synapsis in male and female meiosis. Genes Dev. *13*, 523–531.

Dokshin, G.A., Baltus, A.E., Eppig, J.J., and Page, D.C. (2013). Oocyte differentiation is genetically dissociable from meiosis in mice. Nat. Genet. *45*, 877–883.

Drumond, A.L., Meistrich, M.L., and Chiarini-Garcia, H. (2011). Spermatogonial morphology and kinetics during testis development in mice: a high-resolution light microscopy approach. Reproduction *142*, 145–155.

Endo, T., Romer, K.A., Anderson, E.L., Baltus, A.E., de Rooij, D.G., and Page, D.C. (2015). Periodic retinoic acid-STRA8 signaling intersects with periodic germ-cell competencies to regulate spermatogenesis. Proc. Natl. Acad. Sci. USA *112*, E2347–E2356.

Endoh, M., Endo, T.A., Shinga, J., Hayashi, J., Farcas, A., Ma, K.W., Ito, S., Sharif, J., Endoh, T., Onaga, N., et al. (2017). PCGF6-PRC1 suppresses premature differentiation of mouse embryonic stem cells by regulating germ cell-related genes. eLife *6*, 21064.

Evans, E., Hogarth, C., Mitchell, D., and Griswold, M. (2014). Riding the spermatogenic wave: profiling gene expression within neonatal germ and sertoli cells during a synchronized initial wave of spermatogenesis in mice. Biol. Reprod. *90*, 108.

Feng, J., Liu, T., Qin, B., Zhang, Y., and Liu, X.S. (2012). Identifying ChIP-seq enrichment using MACS. Nat. Protoc. *7*, 1728–1740.

Hamer, G., Gell, K., Kouznetsova, A., Novak, I., Benavente, R., and Höög, C. (2006). Characterization of a novel meiosis-specific protein within the central element of the synaptonemal complex. J. Cell Sci. *119*, 4025–4032.

Hamer, G., Roepers-Gajadien, H.L., van Duyn-Goedhart, A., Gademan, I.S., Kal, H.B., van Buul, P.P., and de Rooij, D.G. (2003). DNA double-strand breaks and gamma-H2AX signaling in the testis. Biol. Reprod. *68*, 628–634.

Handel, M.A., and Schimenti, J.C. (2010). Genetics of mammalian meiosis: regulation, dynamics and impact on fertility. Nat. Rev. Genet. *11*, 124–136.

Hogarth, C.A., Evanoff, R., Snyder, E., Kent, T., Mitchell, D., Small, C., Amory, J.K., and Griswold, M.D. (2011). Suppression of Stra8 expression in the mouse gonad by WIN 18,446. Biol. Reprod. *84*, 957–965.

Ishiguro, K., Kim, J., Fujiyama-Nakamura, S., Kato, S., and Watanabe, Y. (2011). A new meiosis-specific cohesin complex implicated in the cohesin code for homologous pairing. EMBO Rep. *12*, 267–275.

Ishiguro, K., Kim, J., Shibuya, H., Hernández-Hernández, A., Suzuki, A., Fukagawa, T., Shioi, G., Kiyonari, H., Li, X.C., Schimenti, J., et al. (2014). Meiosis-specific cohesin mediates homolog recognition in mouse spermatocytes. Genes Dev. *28*, 594–607.

Jain, D., Puno, M.R., Meydan, C., Lailler, N., Mason, C.E., Lima, C.D., Anderson, K.V., and Keeney, S. (2018). ketu mutant mice uncover an essential meiotic function for the ancient RNA helicase YTHDC2. eLife *7*, 30919.

Kanatsu-Shinohara, M., Ogonuki, N., Inoue, K., Miki, H., Ogura, A., Toyokuni, S., and Shinohara, T. (2003). Long-term proliferation in culture and germline transmission of mouse male germline stem cells. Biol. Reprod. *69*, 612–616.

Kehoe, S.M., Oka, M., Hankowski, K.E., Reichert, N., Garcia, S., McCarrey, J.R., Gaubatz, S., and Terada, N. (2008). A conserved E2F6-binding element in murine meiosis-specific gene promoters. Biol. Reprod. *79*, 921–930.

Kim, J., Ishiguro, K., Nambu, A., Akiyoshi, B., Yokobayashi, S., Kagami, A., Ishiguro, T., Pendas, A.M., Takeda, N., Sakakibara, Y., et al. (2015). Meikin is a conserved regulator of meiosis-I-specific kinetochore function. Nature *517*, 466–471.

Kojima, M.L., de Rooij, D.G., and Page, D.C. (2019). Amplification of a broad transcriptional program by a common factor triggers the meiotic cell cycle in mice. eLife *8*.

Koubova, J., Hu, Y.C., Bhattacharyya, T., Soh, Y.Q., Gill, M.E., Goodheart, M.L., Hogarth, C.A., Griswold, M.D., and Page, D.C. (2014). Retinoic acid activates two pathways required for meiosis in mice. PLoS Genet. *10*, e1004541.

Koubova, J., Menke, D.B., Zhou, Q., Capel, B., Griswold, M.D., and Page, D.C. (2006). Retinoic acid regulates sex-specific timing of meiotic initiation in mice. Proc. Natl. Acad. Sci. USA *103*, 2474–2479.

Lee, J., and Hirano, T. (2011). RAD21L, a novel cohesin subunit implicated in linking homologous chromosomes in mammalian meiosis. J. Cell Biol. *192*, 263–276.

Leseva, M., Santostefano, K.E., Rosenbluth, A.L., Hamazaki, T., and Terada, N. (2013). E2f6-mediated repression of the meiotic Stag3 and Smc1β genes during early embryonic development requires Ezh2 and not the de novo methyltransferase Dnmt3b. Epigenetics *8*, 873–884.

Langmead, B., and Salzberg, S.L. (2012). Fast gapped-read with alignment Bowtie 2. Nat. Methods *9*, 357–359.

Li, H., Handsaker, B., Wysoker, A., Fennell, T., Ruan, J., Homer, N., Marth, G., Abecasis, G., and Durbin, R.; 1000 Genome Project Data Processing Subgroup (2009). The sequence alignment/map format and SAMtools. Bioinformatics *25*, 2078–2079.

Li, X.Z., Roy, C.K., Dong, X., Bolcun-Filas, E., Wang, J., Han, B.W., Xu, J., Moore, M.J., Schimenti, J.C., Weng, Z., et al. (2013). An ancient transcription factor initiates the burst of piRNA production during early meiosis in mouse testes. Mol. Cell *50*, 67–81.

Lin, Y., Gill, M.E., Koubova, J., and Page, D.C. (2008). Germ cell-intrinsic and -extrinsic factors govern meiotic initiation in mouse embryos. Science *322*, 1685–1687.

Liu, C.F., Parker, K., and Yao, H.H. (2010). WNT4/beta-catenin pathway maintains female germ cell survival by inhibiting activin betaB in the mouse fetal ovary. PLoS One *5*, e10382.

Llano, E., Herrán, Y., García-Tuñón, I., Gutiérrez-Caballero, C., de Álava, E., Barbero, J.L., Schimenti, J., de Rooij, D.G., Sánchez-Martín, M., and Pendás, A.M. (2012). Meiotic cohesin complexes are essential for the formation of the axial element in mice. J. Cell Biol. *197*, 877–885.

Mark, M., Jacobs, H., Oulad-Abdelghani, M., Dennefeld, C., Féret, B., Vernet, N., Codreanu, C.A., Chambon, P., and Ghyselinck, N.B. (2008). STRA8-deficient spermatocytes initiate, but fail to complete, meiosis and undergo premature chromosome condensation. J. Cell Sci. *121*, 3233–3242.

Matson, C.K., Murphy, M.W., Griswold, M.D., Yoshida, S., Bardwell, V.J., and Zarkower, D. (2010). The mammalian doublesex homolog DMRT1 is a transcriptional gatekeeper that controls the mitosis versus meiosis decision in male germ cells. Dev. Cell *19*, 612–624.

Menke, D.B., Koubova, J., and Page, D.C. (2003). Sexual differentiation of germ cells in XX mouse gonads occurs in an anterior-to-posterior wave. Dev. Biol. *262*, 303–312.

Mi, H., Muruganujan, A., Ebert, D., Huang, X., and Thomas, P.D. (2019). PANTHER version 14: more genomes, a new PANTHER GO-slim and improvements in enrichment analysis tools. Nucleic Acids Res. *47*, D419–D426.

Miyauchi, H., Ohta, H., Nagaoka, S., Nakaki, F., Sasaki, K., Hayashi, K., Yabuta, Y., Nakamura, T., Yamamoto, T., and Saitou, M. (2017). Bone morphogenetic protein and retinoic acid synergistically specify female germ-cell fate in mice. EMBO J. *36*, 3100–3119.

Mu, W., Starmer, J., Fedoriw, A.M., Yee, D., and Magnuson, T. (2014). Repression of the soma-specific transcriptome by Polycomb-repressive complex 2 promotes male germ cell development. Genes Dev. *28*, 2056–2069.

Murphy, M.W., Lee, J.K., Rojo, S., Gearhart, M.D., Kurahashi, K., Banerjee, S., Loeuille, G.A., Bashamboo, A., McElreavey, K., Zarkower, D., et al. (2015). An ancient protein-DNA interaction underlying metazoan sex determination. Nat. Struct. Mol. Biol. *22*, 442–451.

Nelson, M.A. (1996). Mating systems in ascomycetes: a romp in the sac. Trends Genet. *12*, 69–74.

Oulad-Abdelghani, M., Bouillet, P., Décimo, D., Gansmuller, A., Heyberger, S., Dollé, P., Bronner, S., Lutz, Y., and Chambon, P. (1996). Characterization of a premeiotic germ cell-specific cytoplasmic protein encoded by Stra8, a novel retinoic acid-responsive gene. J. Cell Biol. *135*, 469–477.

Page, S.L., and Hawley, R.S. (2004). The genetics and molecular biology of the synaptonemal complex. Annu. Rev. Cell Dev. Biol. *20*, 525–558.

Picelli, S., Faridani, O.R., Björklund, A.K., Winberg, G., Sagasser, S., and Sandberg, R. (2014). Full-length RNA-seq from single cells using Smart-seq2. Nat. Protoc. *9*, 171–181.

Pittman, D.L., Cobb, J., Schimenti, K.J., Wilson, L.A., Cooper, D.M., Brignull, E., Handel, M.A., and Schimenti, J.C. (1998). Meiotic prophase arrest with failure of chromosome synapsis in mice deficient for Dmc1, a germline-specific RecA homolog. Mol. Cell *1*, 697–705.

Pohlers, M., Truss, M., Frede, U., Scholz, A., Strehle, M., Kuban, R.J., Hoffmann, B., Morkel, M., Birchmeier, C., and Hagemeier, C. (2005). A role for E2F6 in the restriction of male-germ-cell-specific gene expression. Curr. Biol. *15*, 1051–1057.

Quinlan, A.R., and Hall, I.M. (2010). BEDTools: a flexible suite of utilities for comparing genomic features. Bioinformatics *26*, 841–842.

Robert, T., Nore, A., Brun, C., Maffre, C., Crimi, B., Bourbon, H.M., and de Massy, B. (2016). The TopoVIB-Like protein family is required for meiotic DNA double-strand break formation. Science *351*, 943–949.

Romanienko, P.J., and Camerini-Otero, R.D. (2000). The mouse Spo11 gene is required for meiotic chromosome synapsis. Mol. Cell *6*, 975–987.

Schramm, S., Fraune, J., Naumann, R., Hernandez-Hernandez, A., Höög, C., Cooke, H.J., Alsheimer, M., and Benavente, R. (2011). A novel mouse synaptonemal complex protein is essential for loading of central element proteins, recombination, and fertility. PLoS Genet. *7*, e1002088.

Sharov, A.A., Schlessinger, D., and Ko, M.S. (2015). ExAtlas: an interactive online tool for meta-analysis of gene expression data. J. Bioinform. Comput. Biol. *13*, 1550019.

Shibuya, H., Hernández-Hernández, A., Morimoto, A., Negishi, L., Höög, C., and Watanabe, Y. (2015). MAJIN links telomeric DNA to the nuclear membrane by exchanging telomere cap. Cell *163*, 1252–1266.

Shibuya, H., Ishiguro, K., and Watanabe, Y. (2014). The TRF1-binding protein TERB1 promotes chromosome movement and telomere rigidity in meiosis. Nat. Cell Biol. *16*, 145–156.

Sin, H.S., Kartashov, A.V., Hasegawa, K., Barski, A., and Namekawa, S.H. (2015). Poised chromatin and bivalent domains facilitate the mitosis-to-meiosis transition in the male germline. BMC Biol. *13*, 53.

Soh, Y.Q., Junker, J.P., Gill, M.E., Mueller, J.L., van Oudenaarden, A., and Page, D.C. (2015). A gene regulatory program for meiotic prophase in the fetal ovary. PLoS Genet. *11*, e1005531.

Soh, Y.Q.S., Mikedis, M.M., Kojima, M., Godfrey, A.K., de Rooij, D.G., and Page, D.C. (2017). Meioc maintains an extended meiotic prophase I in mice. PLoS Genet. *13*, e1006704.

Sugimoto, A., Iino, Y., Maeda, T., Watanabe, Y., and Yamamoto, M. (1991). Schizosaccharomyces pombe ste11+ encodes a transcription factor with an HMG motif that is a critical regulator of sexual development. Genes Dev. *5*, 1990–1999.

Suzuki, A., Hirasaki, M., Hishida, T., Wu, J., Okamura, D., Ueda, A., Nishimoto, M., Nakachi, Y., Mizuno, Y., Okazaki, Y., et al. (2016). Loss of MAX results in meiotic entry in mouse embryonic and germline stem cells. Nat. Commun. *7*, 11056.

Tedesco, M., La Sala, G., Barbagallo, F., De Felici, M., and Farini, D. (2009). STRA8 shuttles between nucleus and cytoplasm and displays transcriptional activity. J. Biol. Chem. *284*, 35781–35793.

Thorvaldsdóttir, H., Robinson, J.T., and Mesirov, J.P. (2013). Integrative Genomics Viewer (IGV): high-performance genomics data visualization and exploration. Brief. Bioinform *14*, 178–192.

Trapnell, C., Hendrickson, D.G., Sauvageau, M., Goff, L., Rinn, J.L., and Pachter, L. (2013). Differential analysis of gene regulation at transcript resolution with RNA-seq. Nat. Biotechnol. *31*, 46–53.

van Pelt, A.M., and de Rooij, D.G. (1991). Retinoic acid is able to reinitiate spermatogenesis in vitamin A-deficient rats and high replicate doses support the full development of spermatogenic cells. Endocrinology *128*, 697–704.

van Werven, F.J., and Amon, A. (2011). Regulation of entry into gametogenesis. Philos. Trans. R. Soc. Lond., B, Biol. Sci. *366*, 3521–3531.

Vrielynck, N., Chambon, A., Vezon, D., Pereira, L., Chelysheva, L., De Muyt, A., Mézard, C., Mayer, C., and Grelon, M. (2016). A DNA topoisomerase VI-like complex initiates meiotic recombination. Science *351*, 939–943.

Williams, L.H., Fromm, G., Gokey, N.G., Henriques, T., Muse, G.W., Burkholder, A., Fargo, D.C., Hu, G., and Adelman, K. (2015). Pausing of RNA polymerase II regulates mammalian developmental potential through control of signaling networks. Mol. Cell *58*, 311–322.

Wojtasz, L., Cloutier, J.M., Baumann, M., Daniel, K., Varga, J., Fu, J., Anastassiadis, K., Stewart, A.F., Reményi, A., Turner, J.M., et al. (2012).

Meiotic DNA double-strand breaks and chromosome asynapsis in mice are monitored by distinct HORMAD2-independent and -dependent mechanisms. Genes Dev. *26*, 958–973.

Yamaguchi, S., Hong, K., Liu, R., Shen, L., Inoue, A., Diep, D., Zhang, K., and Zhang, Y. (2012). Tet1 controls meiosis by regulating meiotic gene expression. Nature *492*, 443–447.

Yang, F., De La Fuente, R., Leu, N.A., Baumann, C., McLaughlin, K.J., and Wang, P.J. (2006). Mouse SYCP2 is required for synaptonemal complex assembly and chromosomal synapsis during male meiosis. J. Cell Biol. *173*, 497–507.

Yokobayashi, S., Liang, C.Y., Kohler, H., Nestorov, P., Liu, Z., Vidal, M., van Lohuizen, M., Roloff, T.C., and Peters, A.H. (2013). PRC1 coordinates timing of sexual differentiation of female primordial germ cells. Nature *495*, 236–240.

Yoshida, K., Kondoh, G., Matsuda, Y., Habu, T., Nishimune, Y., and Morita, T. (1998). The mouse RecA-like gene Dmc1 is required for homologous chromosome synapsis during meiosis. Mol. Cell *1*, 707–718.

Yoshinaga, K., Nishikawa, S., Ogawa, M., Hayashi, S., Kunisada, T., Fujimoto, T., and Nishikawa, S. (1991). Role of c-kit in mouse spermatogenesis: identification of spermatogonia as a specific site of c-kit expression and function. Development *113*, 689–699.

Zhou, Q., Nie, R., Li, Y., Friel, P., Mitchell, D., Hess, R.A., Small, C., and Griswold, M.D. (2008). Expression of stimulated by retinoic acid gene 8 (Stra8) in spermatogenic cells induced by retinoic acid: an in vivo study in vitamin a-sufficient postnatal murine testes. Biol. Reprod. *79*, 35–42.

Zhu, L.J., Gazin, C., Lawson, N.D., Pagès, H., Lin, S.M., Lapointe, D.S., and Green, M.R. (2010). ChIPpeakAnno: a bioconductor package to annotate ChIP-seq and ChIP-chip data. BMC Bioinformatics *11*, 237.

Zickler, D., and Kleckner, N. (2015). Recombination, pairing, and synapsis of homologs during meiosis. Cold Spring Harb. Perspect. Biol. *7*, a016626.

STAR★METHODS

KEY RESOURCES TABLE

REAGENT or RESOURCE	SOURCE	IDENTIFIER
Antibodies		
Rabbit Anti-PLZF (IF, 1:1000)	Abcam	Cat# ab189849
Rabbit Anti-HA (WB, IF, 1:1000)	Abcam	Cat# ab9110 RRID:AB_307019
Rabbit Anti-H3S10P (IF, 1:2000)	Abcam	Cat# ab5176 RRID:AB_304763
Rabbit Anti-SYCP1 (IF, 1:1000)	Abcam	Cat# ab15090 RRID:AB_301636
Rabbit Anti-γH2AX (IF, 1:1000)	Abcam	Cat# ab11174 RRID:AB_297813
Mouse Anti-γH2AX (IF, 1:1000)	Abcam	Cat# ab26350 RRID:AB_470861
Rabbit Anti-DMC1 (IF, 1:1000)	Santa Cruz	Cat# SC-22768 RRID:AB_2277191
Mouse Anti-DMRT1 (IF, 1:1000)	Santa Cruz	Cat# SC-377167
Rabbit Anti-SOX9 (IF, 1:1000)	Abcam	Cat# ab185230 RRID:AB_2715497
Rabbit Anti-Cyclin A2 (IF, 1:1000)	Abcam	Cat# ab32386 RRID:AB_2244193
Rabbit Anti-Actin (IF, 1:1000)	Cell Signaling Technologies	Cat# 4970 RRID:AB_2223172
Rabbit Anti-GFP (IF, 1:1000) (ChIP, 5μg per 2.5×10^7 Cells)	Abcam	Cat# ab6556 RRID:AB_305564
Rat Anti-TRA98 (IF, 1:1000)	Abcam	Cat# ab82527 RRID:AB_1659152
Rabbit Anti-Mouse MEIKIN (IF, 1:1000)	Kim et al., 2015	N/A
Mouse Anti-Mouse SYCP3 (IF, 1:1000)	Ishiguro et al., 2011	N/A
Rat Anti-Mouse c-Kit (IF, 1:1000)	Yoshinaga et al., 1991	N/A
Rat Anti-Mouse SYCP3 (IF, 1:2000)	This paper	N/A
Guinea Pig Anti-Mouse SYCP3 (IF, 1:2000)	This paper	N/A
Rat Anti-Mouse STRA8 (IF, 1:1000)	This paper	N/A
Rabbit Anti-Mouse STRA8 (IF, 1:1000, WB, 1:1000) (ChIP, 5μg per 3.5×10^7 Cells)	This paper	N/A
Rabbit Anti-Mouse MEIOSIN N-Terminal (a.a. 1–224) (IF, WB, 1:1000) (ChIP, 5μg per 2.5×10^7 Cells)	This paper	N/A
Rat Anti-Mouse MEIOSIN N-Terminal (a.a. 1–224) (IF, 1:500)	This paper	N/A
Guinea Pig Anti-Mouse MEIOSIN N-Terminal (a.a. 1–224) (IF, 1:500)	This paper	N/A
Rabbit Anti-Mouse MEIOSIN C-Terminal (a.a. 405–589) (WB, 1:1000)	This paper	N/A
Rat Anti-Mouse MEIOSIN C-Terminal (a.a. 405–589) (IF, 1:500)	This paper	N/A
Guinea Pig Anti-Mouse MEIOSIN C-Terminal (a.a. 405–589) (IF, 1:500) (ChIP, 5μg per 2.5×10^7 Cells)	This paper	N/A
Anti-HA 12CA5 Monoclonal Antibody (WB, 1:1000) (IP, 5μg per IP of Testes Extract)	Roche	Cat# 11583816001 RRID:AB_514505
Anti-FLAG M2 Monoclonal Antibody Agarose Affinity Gel (IP, 100μl per IP of Testes Extract)	Sigma-Aldrich	Cat# A2220 RRID:AB_10063035
Rabbit Anti-Pan RAR (M-454) (ChIP, 5μg per 2.5×10^6 Cells)	Santa Cruz	Cat# SC-773 RRID:AB_2175398

(*Continued on next page*)

Continued

REAGENT or RESOURCE	SOURCE	IDENTIFIER
Rabbit Anti-H3K4me3 (ChIP, 5μg per 2.5×10^6 Cells)	Abcam	Cat# ab8580 RRID:AB_306649
Rabbit Anti-H3K27me3 (ChIP, 5μg per 2.5×10^6 Cells)	Upstate	Cat# 07–449 RRID:AB_310624
Rabbit Anti-H3K27Ac (ChIP, 5μg per 2.5×10^6 Cells)	Active motif	Cat# 39133 RRID:AB_2561016
Normal Rabbit IgG (ChIP, 5μg per 2.5×10^6 Cells)	Upstate	Cat# 12–370 PRID: AB_145841
Bacterial and Virus Strains		
E. coli strain BL21-CodonPlus(DE3)-RIPL	Agilent	Cat# 230280
Chemicals, Peptides, and Recombinant Proteins		
Ni-NTA Agarose	QIAGEN	Cat# 30210
CNBr-Activated Sepharose	GE healthcare	Cat# 17043001
Tissue-Tek O.C.T. Compound	Sakura Finetek	Cat# 4583
Bovine Serum Albumin	Thermo Fisher Scientific	Cat# 15553027
Win 18,446	Cayman Chemical	Cat#14018
Vectashield Mounting Medium Containing DAPI	Vector Laboratory	Cat# H-1200
Superscript III Reverse Transcriptase	Thermo Fisher Scientific	Cat# 18080044
Trizol Reagent	Thermo Fisher Scientific	Cat# 15596018
Ex-Taq Polymerase	Takara	Cat# RR001B
ECL Prime	GE healthcare	Cat# RPN2232
NuPage 4 %–12 %Bis-Tris Protein Gel	Thermo Fisher Scientific	Cat# NP0322BOX
Silver Quest	Thermo Fisher Scientific	Cat# 6070
Dynabeads Protein A	Thermo Fisher Scientific	Cat# 10002D
Protein A/G PLUS Agarose	Santa Cruz	Cat# sc-2003
3xFLAG Peptide	Sigma-Aldrich	Cat# F4799
Dimethyl Pimelimidate Dihydrochloride (DMP)	Sigma-Aldrich	Cat# D8388
SimplyBlue	Thermo Fisher	Cat# LC6065
Pierce DTT, No-Weight Format (48×7.7mg)	Thermo Fisher Scientific	Cat# 20291
Pierce Iodoacetamide, Single-Use (24×9.3mg)	Thermo Fisher Scientific	Cat# 90034
Trypsin/Lys-C Mix, Journal of Mass Spectrom. Grad (5×20μg)	Promega	Cat# V5073
cOmplete, EDTA-Free	Roche	Cat# 4 693 132
RIPA Buffer	Thermo	Cat# 89900
5-Ethynyl-2′-Deoxyuridine (EdU)	Wako	Cat# 050-08844
All-Trans Retinoic Acid (RA)	Wako	Cat# 188-01113
Pierce 16% Formaldehyde, Methanol Free	Thermo Fisher	Cat# 28906
Disuccinimidyl Glutarate	ProteoChem	Cat# C1140
Disuccinimidyl Glutarate	Thermo Fisher Scientific	Cat# 20593
Collagenase	Sigma-Aldrich	Cat# C0130
DNase II	Sigma-Aldrich	Cat# 8764
Proteinase Inhibitor Cocktail	Sigma-Aldrich	Cat# P8340
Z-VAD-FMK	Calbiochem	Cat# 627610
Ethylene Glycolbis Succinimidyl Succinate	Thermo Fisher Scientific	Cat# 21565
H&E Staining System	Leica	Cat# 3801698
Giemza	Wako	Cat# 079-04391
Cas9 Protein	NIPPON GENE	Cat# 317-08441
UltraPure™ SDS Solution, 10%	Thermo Fisher Scientific	Cat# 15553027
RNase A	MACHERY-NAGEL	Cat# 740505.50
Proteinase K Solution (20 mg/mL)	Thermo Fisher Scientific	Cat# AM2546

(*Continued on next page*)

Continued

REAGENT or RESOURCE	SOURCE	IDENTIFIER
Glycogen	Wako	Cat# 077-05311
Triton X-100	Sigma-Aldrich	Cat# T9284
Superscript II Reverse Transcriptase	Thermo Fisher Scientific	Cat# 18064014
Betaine (BioUltra ≥99.0%)	Sigma-Aldrich	Cat# 61962
RNasin® Plus Ribonuclease Inhibitors	Promega	Cat# N2611
Magnesium Chloride (MgCl2; Anhydrous)	Sigma-Aldrich	Cat# M8266
Critical Commercial Assays		
MEBSTAIN Apoptosis TUNEL Kit Direct	MBL	Cat# 8445
Click-iT EdU Imaging Kit	Thermo Fisher Scientific	Cat# C10086
TruSeq Standard mRNA LT Sample Prep Kit	Illumina	Cat# 20020594
NextSeq 500/550 High Output v2 Kit	Illumina	Cat# 20024906
TruSeq RNA Sample Preparation Kit v2	Illumina	Cat# RS-122-2001
MiSeq Reagent Kit v2	Illumina	Cat# MS-102-2002
MiSeq Reagent Kit v3	Illumina	Cat# MS-102-3001
Illumina ChIP-Seq Sample Prep Kit	Illumina	Cat# FC-102-1003
Illumina Sequencing Kit v4	Illumina	Cat# 15003926
Illumina TruSeq ChIP Sample Preparation Kit	Illumina	Cat# IP-202-1012
Nextera XT Index Kit (24 Indices)	Illumina	Cat# FC-131-1001
Nextera XT DNA Library Prep Kit	Illumina	Cat# FC-131-1024
KAPA Library Preparation Kits	KAPA Biosystems	Cat# KK8221
KAPA HiFi HotStart ReadyMix	KAPA Biosystems	Cat# KK2601
SeqCap Adaptor Kit A	Roche	Cat# 07141530001
SeqCap Adaptor Kit B	Roche	Cat# 07141548001
Deposited Data		
RNA-Seq of WT, *Meiosin* KO and *Stra8* KO Testes	This paper	DDBJ DRA007066,
ChIP-Seq of MEIOSIN and STRA8	This paper	DDBJ DRA007778 DRA009056
SMART-Seq of STRA8-GFP Positive Cells of WT and *Meiosin* KO Testes	This paper	DDBJ DRA008525
RNA-Seq and ChIP-Seq of GS Cells	This paper	GEO GSE116798
DMRT1 ChIP-Seq Data	Murphy et al., 2015	GEO GSE64892
STRA8-FLAG ChIP-Seq Data	Kojima et al., 2019	GEO GSE115928
Experimental Models: Cell Lines		
Ta1 Mouse ES Cells (F1 Hybrid of C57BL/6J × 129S6/SvEvTac)	Amano et al., 2013	N/A
Mouse GS Cells (GS-DG1, Derived from Male Mouse day1 Testis, Strain DBA/2)	Kanatsu-Shinohara et al., 2003	N/A
Experimental Models: Organisms/Strains		
Mouse: *Stra8-3xFLAG-HA-p2A-GFP* Knock-In	This paper	N/A
Mouse: *Meiosin* Knockout	This paper	N/A
Mouse: *Stra8* Knockout	This paper	N/A
Mouse: C57BL/6N	SLC	
Oligonucleotides		
tracrRNA	FASMAC	GE-002
Primers for RT-PCR, Genotyping, SMART-Seq, Genome Editing	See Table S6	N/A
Recombinant DNA		
pX330	Addgene	#44230
pET19b	Novagen	#69677

(*Continued on next page*)

Continued

REAGENT or RESOURCE	SOURCE	IDENTIFIER
pET19b-Gm4969-N	This paper	N/A
pET19b-Gm4969-C	This paper	N/A
pET19b-mSTRA8	This paper	N/A
pKI92 (Stra8 P2A-GFP KI Vector)	This paper	N/A
Software and Algorithms		
STAR Ver.2.6.0A Ver.2.7.0D		https://github.com/alexdobin/STAR
R	The R Project	https://www.r-project.org
Trim Galore! v0.5.0 (Cutadapt v1.16)	NA	http://www.bioinformatics.babraham.ac.uk/projects/trim_galore/
Cutadapt v1.16	NA	https://cutadapt.readthedocs.io/en/stable/
Cuffdiff v 2.2.1.	Trapnell et al., 2013	http://cole-trapnell-lab.github.io/cufflinks/cuffdiff/
ExAtlas	Sharov et al., 2015	https://lgsun.irp.nia.nih.gov/exatlas/
Bowtie2 v2.3.3, v2.3.4.3	Langmead and Salzberg, 2012	http://bowtie-bio.sourceforge.net/bowtie2/index.shtml
SAMtools v1.5, v0.1.19	Li et al., 2009	http://www.htslib.org
Bedtools	Quinlan and Hall, 2010	https://bedtools.readthedocs.io/en/latest/index.html
MACS2 v2.1.1	Feng et al., 2012	https://github.com/taoliu/MACS
Genome Browser IGV	Thorvaldsdóttir et al., 2013	http://meme-suite.org/tools/meme-chip
MEME-ChIP v4.12.0	Bailey, 2011	http://meme-suite.org/tools/meme-chip
ChIPpeakAnno R Package	Zhu et al., 2010	https://www.bioconductor.org/packages/release/bioc/html/ChIPpeakAnno.html
RepeatMasker Version open-4.0.7	NA	http://repeatmasker.org/
Cis-Regulatory Element System (CEAS) v0.9.9.7 (Package Version 1.0.2)	NA	http://liulab.dfci.harvard.edu/CEAS/index.html
Ngsplot (v2.61)	NA	https://github.com/shenlab-sinai/ngsplot
bam2wig v1.5	NA	https://github.com/MikeAxtell/bam2wig
RSEM v1.3.1	NA	https://deweylab.github.io/RSEM/
FASTX Toolkit v0.0.14	NA	http://hannonlab.cshl.edu/fastx_toolkit/
SoftWoRx	GE Healthcare	N/A
CellSens	OLYMPUS	N/A
BZ-X	KEYENCE	N/A
LASX Ver.2	Leica	N/A
Xcalibur	Thermo Fisher Scientific	N/A
Proteome Discoverer Version 1.4	Thermo Fisher Scientific	N/A
Mascot Search Engine Version 2.5	Matrix Science	N/A
PANTHER	Mi et al., 2019	http://pantherdb.org/

LEAD CONTACT AND MATERIALS AVAILABILITY

Further information and requests for resources and reagents should be directed to and will be fulfilled by the Lead Contact, Kei-ichiro Ishiguro (ishiguro@kumamoto-u.ac.jp).

Mouse lines generated in this study have been deposited to Center for Animal Resources and Development (CARD). The antibodies are available upon request. There are restrictions to the availability of antibodies due to the lack of an external centralized repository for its distribution and our need to maintain the stock. We are glad to share antibodies with reasonable compensation by requestor for its processing and shipping. All unique/stable reagents generated in this study are available from the Lead Contact with a completed Materials Transfer Agreement.

EXPERIMENTAL MODEL AND SUBJECT DETAILS

Animals

Meiosin knockout mice were C57BL/6 background. All other knockout and knock-in mice were congenic with the C57BL/6 background. Male mice were used for immunoprecipitation of testis extracts, histological analysis of testes, immunostaining of testes, RNA-seq, and ChIP-seq experiments. Female mice were used for Giemsa staining of oocyte chromosomes, histological analysis of the ovaries, immunostaining experiments. Whenever possible, each knockout animal was compared to littermates or age-matched non-littermates from the same colony, unless otherwise described. Animal experiments were approved by the Institutional Animal Care and Use Committee (approval F28-078, A30-001, A28-026).

METHOD DETAILS

Generation of *Stra8-3xFLAG-HA-p2A-GFP* Knock-In Mouse and Genotyping

The targeting vector was designed to insert 3xFLAG-HA-p2A-EGFP-3'UTR in frame with the coding sequence into the Exon 9 of the *Stra8* genomic locus. Targeting arms of 2.13 kb and 1.10 kb fragments, 5′ and 3′ of the Exon 9 of *Stra8* gene respectively, were generated by PCR from mouse C57BL/6 genomic DNA and directionally cloned flanking p*GK-Neo*-polyA and *DT-A* cassettes. The 5′ arm is followed by nucleotide sequences encoding 3xFLAG, HA, p2A, EGFP and the 3′UTR of *Stra8* gene. Ta1 ES cells (F1 hybrid of C57BL/6J × 129S6/SvEvTac) (Amano et al., 2013) were co-transfected with the targeting vector and pX330 plasmids (Addgene) expressing Crispr-gRNAs directing GCCTCAGGTCACATTATCGG(tgg) and TGCAATCAGTTCCGACTCTC (tgg), which locates at the 3′ region of the Exon 9 of *Stra8* gene. The G418-resistant ES clones were screened for homologous recombination with the *Stra8* locus by PCR using primers

St8-24996F: 5'-AGGCCCAGCATATGTCTAACATCAG-3' and KI96ES-19814R-HA: 5′- GGGCACGTCGTAGGGGTATCCCTTG -3′ for the left arm (3636 bp): neo-F: 5′- GGACCGCTATCAGGACATAGCGTTGGC and St8-33130R: 5′- CCTTCCCAACTCTGTCTGT CCTTTC for the right arm (1738bp).

The homologous recombinant cells were isolated and chimeric mice were generated by aggregation (host ICR) of recombinant ES cells. Chimeric males were mated to C57BL/6N females and the progenies were genotyped by PCR using the primers

St8-24996F: 5'-AGGCCCAGCATATGTCTAACATCAG-3' and St8-29564R: 5'- AGAAGGCTTTTGGAAGCAGCCTTTC-3' for the knock-in allele (4586 bp) and the wild-type allele (3668 bp). Primer sequences are listed in Table S6.

Generation of *Meiosin* Knockout Mice and Genotyping

Meiosin knockout mouse was generated by introducing Cas9 protein (317-08441; Nippon Gene), tracrRNA (GE-002; FASMAC, Kanagawa, Japan), synthetic crRNA (FASMAC) and ssODN into C57BL/6N fertilized eggs using electroporation. For generating *Meiosin* Exon6–14 deletion (Ex6-14Δ) allele, the synthetic crRNAs were designed to direct CAGTTGTGACTAGAGACTAG(tgg) of the *Gm4969* intron 5 and ATGCTTATGGAATTGATACG(tgg) in the 3′-neighboring region of the Exon14. ssODN: gggTGTCAAAGTATAGAAG-CAAAATGCTTATGGAATTGATTTTATTTATTTAGGCAGGCCATAGTCCCACTTCACAGGTATGTGCACT was used as a homologous recombination template.

The electroporation solutions contained [10μM of tracrRNA, 10μM of synthetic crRNA, 0.1 μg/μl of Cas9 protein, ssODN (1μg/μl)] for *Meiosin* knockout in Opti-MEM I Reduced Serum Medium (31985062; Thermo Fisher Scientific). Electroporation was carried out using the Super electroporator NEPA 21 (NEPA GENE, Chiba, Japan) on Glass Microslides with round wire electrodes, 1.0-mm gap (45-0104; BTX, Holliston, MA). Four steps of square pulses were applied (1, three times of 3 mS poring pulses with 97-mS intervals at 30 V; 2, three times of 3-mS polarity-changed poring pulses with 97-mS intervals at 30 V; 3, five times of 50 mS transfer pulses with 50-mS intervals at 4 V with 40% decay of voltage per each pulse; 4, five times of 50-mS polarity-changed transfer pulses with 50-mS intervals at 4 V with 40% decay of voltage per each pulse).

The targeted Ex6-14Δ allele in F0 mice were identified by PCR using the following primers; Gm4969-22787F: 5′-AAGAAGAAGTT TACCCGAGTGTCAG-3′ and Gm4969-29964R: 5′-GAGGTAAAGGGTTTGAGTTCAGACC-3′ for the knockout allele (543 bp) and the wild-type allele (7179 bp). The PCR amplicons were verified by sequencing. Out of 41 F0 founders, 23 mice have *Meiosin* Ex6-14Δ allele (10 mice have a designed sequence derived from ssODN in the mutant allele). For avoiding potential mosaicism of the mutant allele, the F0 mutant founders were backcrossed with C57BL/6 to segregate *Meiosin* Ex6-14Δ allele and establish heterozygous lines. Since homozygous mouse with *Meiosin* Ex6-14Δ allele was infertile both in male and female, mice were maintained as *Meiosin* Ex6-14Δ heterozygous mutant. The *Meiosin* KO (Ex6-14Δ) progenies were genotyped by PCR using Gm4969-22787F, Gm4969-29605F: 5′-CCAGAGAGGAAATGTATTTACTGATCC-3′ and Gm4969-29909R: 5′-GGGTGTCAAAGTATAGAAGCAAAATGC-3′ for the knockout allele (488 bp) and the wild-type allele (305 bp). Primer and synthetic oligonucleotide sequences are listed in Table S6.

Generation of *Stra8* Knockout Mice and Genotyping

Stra8 knockout mice were generated in the context of *Stra8-3xFLAG-HA-p2A-GFP* knock-in allele to facilitate later genotyping. Cas9 protein, tracrRNA (GE-002; FASMAC, Kanagawa, Japan) and synthetic crRNA (FASMAC) were introduced into fertilized eggs of *Stra8-3xFLAG-HA-p2A-GFP* heterozygous. The synthetic crRNA was designed to direct ACAGATCGTCAAAGGTCTCC (agg) in the Exon9 of *Stra8*.

The electroporation was performed as described above, except that solution contained [10 μM of tracrRNA, 10 μM crRNA and 0.1 μg/μl of Cas9 protein] for *Stra8* knockout.

The targeted alleles of F0 mice were amplified by PCR using the following primers, Stra8 wt F3: 5′-CTGGAGTGTGAAGCC CACCTGGGATG-3′ and gfp R2: 5′-AGCTCCTCGCCCTTGCTCACCATAG-3′. The PCR amplicons were cloned into pCRII-TOPO and sequenced. F0 mice were backcrossed with C57BL/6N to segregate the mutant allele (*Stra8* ^{Ex9}) and the progenies were genotyped by PCR using St8-24996F: 5′-AGGCCCAGCATATGTCTAACATCAG-3′ and St8-29564R: 5′- AGAAGGCTTTTGGAAG-CAGCCTTTC-3′ for the knockout allele (4586 bp) and the wild-type allele (3668 bp). Four mouse lines with a different *Stra8* ^{Ex9} mutant allele were established, of which homozygous (*Stra8*^{Ex9} KO) mice show essentially same phenotype. Primer and synthetic oligonucleotide sequences are listed in Table S6.

WIN 18,446 and Retinoic Acid Treatment

Neonatal male mice were injected subcutaneously with 100 μl of 10 mg/ml WIN 18,446 (5% DMSO/95% corn oil, Cayman Chemical) daily during 5dpp-11dpp to block spermatogonial differentiation and meiosis. At 12dpp, mice receiving consecutive WIN 18,446 treatments were injected intraperitoneally with 100 μl of 2.5 mg/ml all-trans retinoic acid (RA) (10% DMSO/90% corn oil) or with carrier control, followed by testes collection at 13dpp. For ChIP-seq analyses, mice received daily injections of WIN 18,446 during 3dpp-13dpp. At 14dpp, mice were treated with RA, followed by testes collection 8 days after the treatment.

EdU Labeling of Mouse Seminiferous Tubules

Male mice (8-week-old) were injected intraperitoneally with 100 μl of 2 mg/ml EdU (Wako). Testes were collected 2 or 24 hours after the injection. EdU-incorporated cells on the seminiferous tubule sections were envisioned using a Click-iT EdU imaging kit (Thermo Fisher).

Preparation of Testis Extracts

Testis chromatin-bound and -unbound extracts were prepared as described previously(Ishiguro et al., 2011). Briefly, testicular cells were suspended in low salt extraction buffer (20 mM Tris-HCl [pH 7.5], 100 mM KCl, 0.4 mM EDTA, 0.1% TritonX100, 10% glycerol, 1 mM β-mercaptoethanol) supplemented with Complete protease Inhibitor (Roche). After homogenization, the soluble chromatin-unbound fraction was separated after centrifugation at 100,000*g* for 30 min. The chromatin bound fraction was extracted from the insoluble pellet by high salt extraction buffer (20 mM HEPES-KOH [pH 7.0], 400 mM KCl, 5 mM $MgCl_2$, 0.1% Tween20, 10% glycerol, 1 mM β-mercaptoethanol) supplemented with Complete protease Inhibitor. The solubilized chromatin fraction was collected after centrifugation at 100,000*g* for 30 min at 4°C.

Immuno-Affinity Purification

Immuno-affinity purification was performed with anti-FLAG M2 monoclonal antibody-coupled magnetic beads (Sigma-Aldrich) from the testis chromatin-bound and -unbound fractions of *Stra8-3xFLAG-HA-p2A-GFP* knock-in mice (10 to 12-day-old). For negative control, mock immuno-affinity purification was done from the testis chromatin-bound and -unbound fractions from the age-matched wild type mice. The beads were washed with high salt extraction buffer for chromatin-bound proteins and low salt extraction buffer for chromatin-unbound proteins. The anti-FLAG-bound proteins were eluted by 3xFLAG peptide (Sigma-Aldrich). The second immuno-affinity purification was performed anti-HA 12CA5 monoclonal antibody (Roche)-coupled Sepharose. The bead-bound proteins were eluted with 40 μl of elution buffer (100-mM glycine-HCl [pH 2.5], 150 mM NaCl), and then neutralized with 4 μl of 1 M Tris-HCl [pH 8.0].

For conventional immunoprecipitation of endogenous STRA8 from chromatin fraction, 5 μg of affinity-purified rabbit anti-STRA8 (derived from 2 different immunized animals, Ab.1, and Ab.2) and control rabbit IgG antibodies were crosslinked to 50 μl of protein A-Dynabeads (Thermo Fisher) by DMP (Sigma). The antibody-crosslinked beads were added to the testis chromatin-bound and -unbound extracts prepared from wild type testes (10 to 14-day-old). The beads were washed as described above. The bead-bound proteins were eluted as described above. The immunoprecipitated proteins were run on 4 %–12 % NuPage (Thermo Fisher) in MOPS-SDS buffer and silver-stained with Silver Quest (Thermo Fisher), immunoblotted or analyzed by LC-MS/MS. Immunoblot image was developed using ECL prime (GE Healthcare) and captured by LAS4000mini (GE Healthcare) or Fusion Solo (VILBER).

Mass Spectrometry

The immunoprecipitated proteins were run on 4 %–12 % NuPage (Thermo Fisher) by 1 cm from the well and stained with SimplyBlue (Thermo Fisher) for the in-gel digestion. The gel containing proteins was excised, cut into approximately 1mm sized pieces. Proteins in the gel pieces were reduced with DTT (Thermo Fisher), alkylated with iodoacetamide (Thermo Fisher), and digested with trypsin and lysyl endopeptidase (Promega) in a buffer containing 40-mM ammonium bicarbonate, pH 8.0, overnight at 37°C. The resultant peptides were analyzed on an Advance UHPLC system (AMR/Michrom Bioscience) coupled to a Q Exactive mass spectrometer (Thermo Fisher) processing the raw mass spectrum using Xcalibur (Thermo Fisher Scientific). The raw LC-MS/MS data was analyzed against the NCBI non-redundant protein/translated nucleotide database restricted to *Mus musculus* using Proteome Discoverer version 1.4 (Thermo Fisher) with the Mascot search engine version 2.5 (Matrix Science). A decoy database comprised of either randomized or reversed sequences in the target database was used for false discovery rate (FDR) estimation, and Percolator algorithm was used to evaluate false positives. Search results were filtered against 1% global FDR for high confidence level.

PCR with Reverse Transcription

Total RNA was isolated from tissues and embryonic gonads using Trizol (Thermo Fisher). cDNA was generated from total RNA using Superscript III (Thermo Fisher) followed by PCR amplification using ex-Taq polymerase (Takara) and template cDNA. Sequences of primers used to generate RT-PCR products from cDNA are as follows:

GAPDH-F: 5′-TTCACCACCATGGAGAAGGC-3′
GAPDH-R: 5′-GGCATGGACTGTGGTCATGA-3′
Meiosin-1842F: 5′-GATGAACCGGAAGCAGTACATCCG-3′
Meiosin-2124R: 5′-TCACTGGCAGTTAGGGGTGGGCAG-3′
Stra8-749F: 5′-GGCAGACTCTCTCTGAGGAGAAAA-3′
Stra8-1122R: 5′-CTCTGGTTCCTGGTTTAATGGAGT-3′

Primer sequences are listed in Table S6.

Antibodies

The following antibodies were used for immunoblot (IB) and immunofluorescence (IF) studies: rabbit anti-PLZF (IF, 1:1000, Abcam: ab189849), rabbit anti-HA (IB, IF, 1:1000, Abcam: ab9110), rabbit anti-H3S10P (IF, 1:2000, Abcam: ab5176), rabbit anti-SYCP1 (IF, 1:1000, Abcam ab15090), rabbit anti-γH2AX (IF, 1:1000, Abcam ab11174), mouse anti-γH2AX (IF, 1:1000, Abcam ab26350), rabbit anti-CyclinA2 (IF, 1:1000, Abcam ab32386), rabbit anti-DMC1 (IF, 1:1000, Santa Cruz: SC-22768), mouse anti-DMRT1 (IF, 1:1000, Santa Cruz: SC-377167), rabbit anti-MEIKIN (Kim et al., 2015), mouse anti-SYCP3 (Ishiguro et al., 2011), rabbit anti-actin (IB, 1:1000, CST #4970), rabbit anti-GFP (IF, 1:1000, ab6556), rat anti-TRA98 (IF, 1:1000, ab82527), rabbit anti-SOX9 (IF, 1:1000, Abcam ab185230), rat anti-cKit (IF, 1:1000) (Yoshinaga et al., 1991).

Antibody Production

Polyclonal antibodies against mouse STRA8 (a.a. 1–393) were generated by immunizing rabbits and rats. Polyclonal antibodies against mouse MEIOSIN N-terminal (a.a. 1–224) and C-terminal (a.a. 405–589) were generated by immunizing rabbits, rats and guinea pigs. Polyclonal antibodies against mouse SYCP3 were generated by immunizing rats and guinea pigs. All His-tagged recombinant proteins were produced by inserting cDNA fragments in-frame with pET19b (Novagen) in *E. coli* strain BL21-CodonPlus(DE3)-RIPL (Agilent), solubilized in a denaturing buffer (6 M HCl-guanidine, 20 mM Tris-HCl [pH 7.5]) and purified by Ni-NTA (Qiagen) under denaturing conditions. The antibodies were affinity-purified from the immunized serum with immobilized antigen peptides on CNBr-activated Sepharose (GE Healthcare).

Histological Analysis

For immunofluorescence staining, testes and embryonic ovaries were embedded in Tissue-Tek O.C.T. compound (Sakura Finetek) and frozen at -80°C. Cryosections were prepared on the MAS-GP typeA-coated slides (Matsunami) at 8–10-μm thickness, and then air-dried and fixed in 4% paraformaldehyde in PBS at pH 7.4. For CCNA2 and GFP immuno-staining, cryosections were prepared after fixing testes in 4% paraformaldehyde. For whole mount immunostaining, seminiferous tubules were fixed in 4% paraformaldehyde in PBS for 1hours, and sequentially dehydrated in 25%–100% methanol containing 0.04% Tween20. For, hematoxylin and eosin staining, testes, epididymis and ovaries were fixed in 10% formalin and embedded in paraffin. Sections were prepared on MAS-GP typeA-coated slides (Matsunami) at 6-μm thickness. The slides were dehydrated and stained with hematoxylin and eosin.

Immunofluorescence Microscopy of Testis and Ovary

The serial sections of frozen testes and embryonic ovaries were fixed in 4% PFA for 5 min at room temperature and permeabilized in 0.1% TritonX100 in PBS for 10 min. The sections were blocked for 10 min in PBS, 3% BSA, and incubated at room temperature with the primary antibodies in a blocking solution. After three washes in PBS, the sections were incubated for 1 hrs at room temperature with Alexa-dye-conjugated secondary antibodies (1:1000; Invitrogen) in a blocking solution. TUNEL assay was performed using MEBSTAIN Apoptosis TUNEL Kit Direct (MBL 8445). DNA was counterstained with Vectashield mounting medium containing DAPI (Vector Laboratory).

Imaging

Immunostaining images were captured with DeltaVision (GE Healthcare). The projection of the images was processed with the softWoRx software program (GE Healthcare). Immunostaining images of cKit positive cells were captured with confocal microscope TSC SP8 and processed with LASX ver.2 Software (Leica). All images shown were Z-stacked. For counting seminiferous tubules, immunostaining images were captured with BIOREVO BZ-X710(KEYENCE), and processed with BZ-H3A program. Bright field images were captured with Olympus BX53 fluorescence microscope and processed with CellSens standard program.

Chromatin Immunoprecipitation

To enrich preleptotene spermatocytes, male mice were daily injected with WIN 18,446 during 3dpp-13dpp, followed by RA injection at 14dpp and testes collection 8 days after the treatment. Assessment by immunostaining of the seminiferous tubules indicated that

samples contained 78.9% of STRA8+/MEIOSIN+ preleptotene spermatocytes, and 11.1% of STRA8+ spermatogonia. The seminiferous tubules were minced and digested with 100 μg/ml collagenase and 0.5 units/ml DNase II, followed by filtration through a 40-μm cell strainer (Falcon). Testicular cells were fixed in 1% formaldehyde (Thermo Fisher)/2mM disuccinimidyl glutarate (ProteoChem) in PBS for 10 minutes at room temperature. Crosslinked cells were lysed with LB1 (50 mM HEPES pH 7.5, 140 mM NaCl, 1 mM EDTA, 10% glycerol, 0.5% NP-40, and 0.25% Triton X-100) and washed with LB2 (10 mM Tris-HCl pH 8.0, 200 mM NaCl, 1 mM EDTA, 0.5 mM EGTA). Chromatin lysates were prepared in RIPA buffer (Thermo 89900; 25 mM Tris-HCl pH7.6, 150 mM NaCl, 0.1% SDS, 1% NP-40, 1% sodium deoxycolate, proteinase inhibitor cocktail), by sonication with Covaris S220 (Peak Incident Power, 175: Acoustic Duty Factor, 10%: cycle Per Burst, 200: treatment time, 600sec: cycle, 6).

ChIP was performed using preleptotene enriched spermatocytes. STRA8 ChIP was performed using chromatin lysates equivalent to 3.5×10^7 cells in RIPA buffer, protein A Dyna-beads (Thermo Fisher) coupled with 5 μg of rabbit anti-STRA8 antibody. MEIOSIN ChIP was performed using chromatin lysates equivalent to 2.5×10^7 cells in RIPA buffer, protein A Dyna-beads coupled with 5 μg of rabbit anti-MEIOSIN-N (MEIOSIN ChIP replicate1) or 5 μg of gunia pig anti-MEIOSIN-C (MEIOSIN ChIP replicate2) antibodies. The negative control GFP ChIP was performed using chromatin lysates equivalent to 2.5×10^7 cells in RIPA buffer, protein A Dyna-beads coupled with 5 μg of rabbit anti-GFP antibody.

After 4 hours of incubation at 4°C, beads were washed 4 times in a low salt buffer (20 mM Tris-HCl (pH 8.0), 0.1% SDS, 1% (w/v) TritonX-100, 2 mM EDTA, 150 mM NaCl), and two times with a high salt buffer (20 mM Tris-HCl (pH 8.0), 0.1% SDS, 1% (w/v) TritonX-100, 2 mM EDTA, 500 mM NaCl). Chromatin complexes were eluted from the beads by agitation in elution buffer (10 mM Tris-HCl (pH 8.0), 300 mM NaCl, 5 mM EDTA, 1% SDS) and incubated overnight at 65°C for reverse-crosslinking. Eluates were treated with RNase A and proteinase K, and DNA was ethanol precipitated.

For RAR and histone ChIP, GS cells transduced with *Bax* shRNA lentivirus vectors or cultured in the presence of Z-VAD-FMK (Calbiochem) were treated with or without 100 nM RA for indicated days and fixed in 2 mM disuccinimidyl glutarate, 1.5 mM ethylene glycolbis succinimidyl succinate (Pierce) in PBS followed by 1% formaldehyde for RAR, in 0.5% formaldehyde in PBS for H3K4me3 and H3K27me3, and in 1% formaldehyde in PBS for H3K27Ac. Chromatin lysates were prepared by sonication with Covaris S220 for RAR and H3K27Ac, and by detergent lysis, centrifugal nuclear enrichment and MNase treatment for H3K4me3 and H3K27me3. ChIP was performed using anti-pan RAR (Santa Cruz sc-773), anti-H3K4me3 (**Abcam** ab8580), anti-H3K27me3 (Upstate 07-449) and anti-H3K27Ac (Active Motif 39133) antibodies and elutes were treated as described above. Detailed protocols for ChIP in GS cells are available at Gene Expression Ominibus (GEO) under the accession GSE116798.

Sequencing

For RNA-seq of WT, *Meiosin* KO and *Stra8* KO testes, total RNAs were prepared by Trizol (Thermo Fisher) and quality of total RNA was confirmed by BioAnalyzer 2100 (RIN > 9)Library DNAs were prepared according to the Illumina TruSeq protocol using TruSeq Standard mRNA LT Sample Prep Kit (Illumina) and sequenced by Illumina NextSeq 500 (Illumina) using NextSeq 500/550 High Output v2 Kit (Illumina) to obtain single end 75 nt reads.

For RNA-seq of GS, ES and primary embryonic fibroblast (PEF) cells, libraries were prepared using TruSeq RNA Sample Preparation Kit v2 and sequenced by MiSeq (Illumina) with MiSeq Reagent Kit v2 to obtain paired end 150 nt reads.

For MEIOSIN and STRA8 ChIP-seq, libraries were prepared using 20 ng of input DNA, and 2 ng of MEIOSIN ChIP DNA and 4 ng of STA8 ChIP DNA with KAPA Library Preparation Kit (Kapa Biosystems) and Nimblegen SeqCap Adaptor Kit A or B (Roche) and sequenced by Illumina NextSeq 500 to obtain single end 75 nt reads in the same way as RNA-seq.

For ChIP-seq of GS cells, libraries were prepared using Illumina ChIP-seq sample prep kit and sequenced by GAIIX (Illumina) with Illumina Sequencing kit v4 to obtain single end 36 nt reads for RAR, H3K4me3 and H3K27me3 and using Illumina TruSeq ChIP Sample Preparation Kit and sequenced by MiSeq with MiSeq Reagent Kit v2 to obtain paired end 150 nt reads for H3K27Ac.

Sequencing data are available at DDBJ Sequence Read Archive (DRA) under the accession DRA007066, DRA007778, DRA009056 for RNA-seq of WT, *Meiosin* KO and *Stra8* KO testes and ChIP-seq of MEIOSIN and STRA8. DRA008525 for SMART-seq of STRA8-GFP positive cells of WT and *Meiosin* KO testes. RNA-seq and ChIP-seq of GS cells are available at GEO under the accession GSE116798.

RNA-Seq Data Analysis

Resulting reads were aligned to the mouse genome (GRCm38.89) using STAR ver.2.6.0a after trimmed to remove adapter sequence and low-quality ends using Trim Galore! v0.5.0 (cutadapt v1.16). Gene expression level measured as FPKM was determined with Cuffdiff v 2.2.1 (Trapnell et al., 2013). GTF file was derived from GRCm38.92. Differential expression analysis, principal component analysis and GO-term analysis were performed using ExAtlas website (Sharov et al., 2015) (https://lgsun.irp.nia.nih.gov/exatlas/). As a control dataset, same number of randomized genes that were extracted from whole mouse genes were used.

ChIP-Seq Data Analysis

ChIP-seq reads were trimmed to remove adapter sequence and low-quality ends using Trim Galore! v0.4.3 (cutadapt v.1.15). The trimmed ChIP-seq reads ware mapped to the UCSC mm10 genome assemblies using Bowtie2 v2.3.3 (Langmead and Salzberg, 2012) with default parameters. The resulting SAM files were converted to the BAM format using SAMtools v1.5 (Li et al., 2009). Peak calling was performed using MACS2 v2.1.1. (Feng et al., 2012) with input DNA as a control including a *q*-value cutoff of 0.0001 for STRA8 ChIP-seq, MEIOSIN ChIP-seq (replicate 1 and 2), GFP-ChIP-seq in RIPA buffer. Overlapping ChIP peaks were

intersected by bedtools. Those overlapping with control IgG ChIP peaks were removed by bedtools -v option. The distance to the nearest transcription start site (TSS) and gene feature of the peaks were obtained from Ensembl mouse annotation data using the ChIPpeakAnno (Zhu et al., 2010) and biomaRt R packages. The nearest genes were assigned regardless of distance from the protein binding peaks. Protein binding sites were shown along with genomic loci from Ensembl on the genome browser IGV (Thorvaldsdóttir et al., 2013).

Motif identification was performed using MEME-ChIP v4.12.0 website (http://meme-suite.org/tools/meme-chip) (Bailey, 2011). The sequence of whole ChIP peak length was obtained from UCSC mm10 whole genome annotation data using the ChIPpeakAnno R package, and masked for repetitive elements using RepeatMasker version open-4.0.7. The motif database chose "JASPAR Vertebrates and UniPROBE Mouse".

GO-term analyses were performed from the input of the nearest genes using Gene Ontology Consortium website (http://www.geneontology.org). As a control dataset, same number of randomized genes that were extracted from whole mouse genes were used. ChIP binding regions were annotated with BED file (Quinlan and Hall, 2010) using Cis-regulatory Element System (CEAS) v0.9.9.7 (package version 1.0.2), in which the gene annotation table was derived from UCSC mm10. Average profile and heatmaps for each sample against the dataset of 2439 MEIOSIN-STRA8 common target genes were made using ngsplot (v2.61).

DMRT1 ChIP-seq data were downloaded from GEO with accession number GSE64892 (Murphy et al., 2015). FLAG ChIP-seq data in *Stra8-FLAG* knockin mice (Kojima et al., 2019) were downloaded from GEO GSE115928.

SMART-Seq2 Analysis

GFP positive cells (100 cells) from *Stra8-3xFLAG-HA-p2A-GFP* knock-in male testis were directly sorted in Lysis buffer using SH800S cell sorter (SONY). cDNA was amplified according to Smart-seq2 methods (Picelli et al., 2014). Library DNAs were prepared using Nextera XT Library prep kit (Illumina) and sequenced by NextSeq 500 as described above in RNA-seq sequencing methods. Resulting reads were mapped on mouse genome (GRCm38.93) and gene expression levels were measured by RSEM v1.3.1 after trimmed to removed adaptor sequence and low-quality ends using Trim Galore! v0.5.0 (cutadapt v1.16) and FASTX Toolkit v0.0.14. Differential expression analysis was done by -run-ebseq option of RSEM and GO-term analysis was performed using PANTHER (Mi et al., 2019) with mouse MGI ontology annotations. As a control dataset, same number of randomized genes that were extracted from whole mouse genes were repeatedly (10 times) tested in GO-term analysis that covers 52638 mouse reference genes.

CAGE-Seq

CAGE data were downloaded from GEO with accession number GSE44690. Downloaded fastq file was trimmed to remove adapter sequence and low-quality ends using Trim Galore! v0.4.3 (cutadapt v1.15). The trimmed reads ware mapped on the mouse genome GRCm38.92 using TopHat (v2.1.1), using GTF file (-G (−GTF) GRCm38.92) with option of -g (−max-multihits) 1.

In Vitro Oocyte Culture and Giemsa Staining of Metaphase Chromosome Spread

Ovaries collected from 4-week-old female mice were used after 46 to 48 hrs of treatment with 5 IU of pregnant mare serum gonadotropin. GV oocytes from WT, and oocyte-like cells from *Meiosin* KO were isolated by puncturing the follicles in M2 medium (Sigma). The GV oocytes and GV oocyte-like cells were cultured in M16 medium (Sigma) in a 5% CO_2 atmosphere at 37°C for 5–6hours. For Giemsa staining of metaphase chromosome spread, oocytes and oocyte-like cells were exposed to 0.5% Pronase (Sigma) to remove the zona pellucida, and treated in hypotonic buffer containing 1% sodium citrate/0.1% PVA for 15min. The oocytes and oocyte-like cells were placed on the slides, fixed in the Carnoy's Fixative (75 % methanol, 25% acetic acid) and, stained in 3% Giemsa solution for 30min.

GS Cell Culture

GS cells (kindly provided by Dr. Takashi Shinohara) were cultured on mitomycin C treated mouse primary embryonic fibroblast cells in StemPro-34 medium (Invitrogen) supplemented with StemPro supplement, 50 μg/ml insulin (Wako), 100 μg/ml transferrin, 60 μM putrescine, 30 nM sodium selenite, 6 mg/ml D(+)glucose, 1.8 mM sodium pyruvate, 1 μl/ml DL-lactic acid, 2 mM L-glutamine, 5×10^{-5} M 2-mercaptoethanol, 10^{-4} M ascorbic acid, 10 μg/ml d-biotin, 30 ng/ml β-estradiol, 60 ng/ml progesterone (Sigma), 5 mg/ml bovine albumin (MP Biomedicals), 1 x MEM vitaminE solution, 1 × MEM nonessential amino acids solution, penicillin + streptomycin, 1% fetal calf serum, 10 ng/ml human bFGF, 15 ng/ml rat GDNF (PeproTech, Rocky Hill, NJ, United States of America). All trans retinoic acid was added to the culture medium at a concentration of 10^{-7} M for the indicated duration in the presence of 50 μM Z-VAD-FMK (Calbiochem) to suppress apoptosis.

QUANTIFICATION AND STATISTICAL ANALYSIS

All Statistical analysis was performed using GraphPad Prism.

Figure 2I The seminiferous tubules containing SYCP3+ spermatocyte or spermatocyte-like cells were counted in WT (p10 : n=2, p18 : n=4, 8W : n=4), *Meiosin* KO (p10 : n=2, p18 : n=3, 8W : n=5) and *Stra8* KO (p10 : n=1, p18 : n=4, 8W : n=5) testes. Bar graph indicates mean with SD.

Figure 3A The seminiferous tubules that have H3S10P+/SYCP3+ cells were counted in WT (p10: n=2, p18: n=4, 8W: n=4), *Meiosin* KO (p10: n=2, p18: n=3, 8W: n=5) and *Stra8* KO (p10: n=1, p18: n=4, 8W: n=5) testes. Bar graph indicates mean with SD.

Figure 3D The seminiferous tubules that have H3S10P+/EdU+ spermatocyte-like cells and all the seminiferous tubules that have EdU labeled spermatocyte-like cells were counted in WT (n=1), *Meiosin* KO (n=1) and *Stra8* KO (n=1) testes.

Figure 3G The seminiferous tubules that have TUNEL+ cells were counted in WT (n=3) and *Meiosin* KO (n=3) testes. Bar graph indicates mean with SD.

Figure 4C Numbers of DMC1 foci on SYCP3 axes were counted in WT leptotene, zygotene, pachytene (n = 32, 21, 20 respectively), *Meiosin* KO (n = 32) and *Stra8* KO (n = 56) spermatocytes (-like cells). Number of foci was indicated in the scatter plot with median. p-value (Mann-Whitney t-test) is shown.

DATA AND CODE AVAILABILITY

All data supporting the conclusions are present in the paper and the supplementary materials. Sequencing data for the mouse *Meiosin* gene are deposited in the National Center for Biotechnology Information-National Institutes of Health (NCBI-NIH) GenBank under accession numbers LC371381. The ChIP-seq and RNA-seq data of mouse testes are deposited in the DDBJ Sequence Read Archive (DRA) under accession number DRA007066, DRA007778, DRA009056. SMART-seq data is deposited under DRA008525. Data for RNA-seq and ChIP-seq of GS cells are available at GEO under the accession GSE116798. Mouse lines generated in this study have been deposited to Center for Animal Resources and Development (CARD), *Meiosin* mutant mouse (ID 2555), *Stra8* mutant mouse (ID 2647) and *Stra8-3xFLAG-HA-p2A-GFP* knock-in mouse (ID 2743).